Phil. Trans. R. Soc. Lond. A **309**, 295–314 (1983)
Printed in Great Britain

The application of satellite imaging radars over land to the assessment, mapping and monitoring of resources

By P. H. A. Martin-Kaye and G. M. Lawrence
Hunting Geology and Geophysics Limited, Elstree Way, Borehamwood, Herts. WD6 1SB, U.K.

[Plates 1–12]

Airborne imaging radars have been put to substantial civilian use over the past 15 years, accumulating aggregate areal ground coverage of imagery of about 18×10^6 km^2. Much of this coverage has been from cloud-ridden equatorial regions that pose difficulties for systematic air photography, capitalizing upon radar's capacity to acquire data virtually without regard to daylight and cloud conditions. The work was required mainly for regional development, land-use studies, petroleum and mineral exploration or geothermal energy studies, and was carried out by a few established groups.

The Seasat SAR, operating in 1978, had a coverage essentially restricted to North America and Europe. Although not particularly suited to overland purposes it introduced many additional users to regional radar imagery. The Shuttle imaging radar SIR-A, which flew in November 1981, achieved a coverage of about 10^7 km^2 in the aggregated 8 h of operation, looking at a greater variety of terrain, particularly among arid lands, and geologic type than had been accumulated previously. Examples presented here show the even illumination of SIR-A, and a depiction of geographic and geological features superior to Seasat and in some cases superior to Landsat. Interpretability for regional geological purposes is good and is adequate for general land use and other purposes. In arid regions new applications for studies on desertification and hydrogeology are highlighted. An example of subsurface backscatter is presented. Once wide-covering multifrequency and multitemporal radar become available from N.A.S.A.'s SIR-B and SAMEX, planned for 1984 and 1987 respectively, and from other major radar satellites to be launched by the European Space Agency, the Canadian Centre of Remote Sensing and the Japanese Space Agency, and from the German Spacelab SAR, spaceborne radar imagery will join Landsat as a primary tool in thematic mapping of large areas of the Earth's surface.

1. Introduction

Imaging radars are unaffected by conditions of daylight, haze and most cloud, any of which can defeat scanners and cameras. The images from survey programmes are interpretable to various levels: for general cartography, terrain morphology, land use, natural vegetation and geology; for ice, and sea states; and for other similar purposes. The combination of operational reliability and practical application led to some 18×10^6 km^2 of coverage by commercial airborne mapping radars (SLAR) between 1969 and the present. In 1978 N.A.S.A.'s ocean-monitoring satellite, Seasat, in little over 100 days, inspected about 10^8 km^2 by radar, both over land and sea. In November 1981, the Space Shuttle Columbia obtained radar images of about 10^7 km^2, about 6×10^6 km^2 of which were over land, with the SIR-A (Shuttle Imaging Radar) instrument.

The SLAR surveys were flown widely about the world but emphasized the cloud-ridden tropics. Seasat's recovered data were restricted to the European and North American areas

whereas the Shuttle's radar looked at a great diversity of terrain in the tropics and the near-tropics including, very importantly as it transpired, arid regions. Both the side-looking airborne radar (SLAR) programmes and the imaging from space have shown that radars have valuable resource mapping and monitoring roles to fulfil.

2. Resource surveys by side-looking airborne radar (SLAR)

The principal commercial side-looking radar systems and their surveys for resource evaluations are listed in table 1. Commercial activities were triggered off by the two-stage Project RAMP (Radar Mapping of Panama) in 1967 and 1969, which publicized mapping radar's ability to recover data from clouded areas. Later, the RADAM project covered the Amazon basin and then, in Projecto RADAM BRASIL, the whole of Brazil. Similar operations spread in South America and extended to southeast Asia and to Africa. A comparatively recent review of the developing use of SLAR has been given by McDonald (1980).

The large SLAR programmes of the 1970s were contracted by Governments for thematic interpretative mapwork in the guidance of development planning. Surveys were also commissioned by mining and especially oil companies needing quick initial reconnaissance of remote areas. Nuclear and geothermal power plant siting studies brought about some imaging in North America, Japan and the Philippines. The requirements of oil exploration and the monitoring of ice and the movement of ice flows resulted in substantial use of radar off northern Canada and Alaska.

The characteristics and economics of the commercial SLAR systems operating before the launch of Seasat (1978) dictated that the principal applications were to large-area surveys for 1:200 000–1:250 000 scale image and cartographic products of poorly mapped, logistically and photographically difficult regions. For semi-detailed inventory and monitoring purposes the systems worked well. The reliability of data acquisition allowed fixed-price, fixed-schedule programmes. The images were able to provide an up-to-date pictorial mosaic map which, for numbers of operational purposes, was often much better than had previously existed. The shadowing effects given to landscape by the oblique illumination enabled comparatively ready interpretation of geological structures that are often reflected in morphology. Although the resolution was low (mostly 10–40 m), for the detail required in land-use and natural vegetation mapwork it was sufficient for the mapping scales that are adopted for regional surveys.

A substantial literature on airborne radar imaging and the interpretation of imagery exists. Bibliographies include Bryan (1973, 1979), Moore *et al.* (1974) and Walter (1968). The major SLAR projects are, however, not all well documented publicly, the data of several being unpublished or in summaries. Wing (1971), Wing & Dellwig (1970) and Wing & MacDonald (1973) give accounts of RAMP. The imagery of the Brazilian projects is available with a series of 1:500 000 scale interpretative maps in geology, land use and natural vegetation, together with accompanying reports; general accounts have been given by Azevedo (1971), Moreira (1973) and Correa (1980). A five-volume report (Diazgrandados 1979) has been issued for the PRORADAM project of Columbia. Martin-Kaye & Williams (1973) presented a summary of the radar-geological mapwork for Nicaragua, and Parry & Trevett (1979) and Hunting Technical Services Limited (1978) discussed the land-use and natural vegetation work of the NIRAD project in Nigeria. From a more recent programme in Africa, Dellwig (1980) describes the updating of maps of Togo. Of other regional programmes, e.g. Peru (see, for example,

TABLE 1. COMMERCIAL SLAR SYSTEMS

(A full list of operating SLAR systems is given in Schlude (1981).)

operator	equipment	type	radar wavelength	signal polarization	image swath km	nominal resolution/m along track (range)	nominal resolution/m across track (azim.)	platform	areas covered
Westinghouse	Westinghouse AN/APQ-97	real aperture	Ka; 0.86 cm	HH, HV	21	25	8	DC6 B	*ca.* 1.7×10^6 km² over North America, Panama (RAMP), Colombia, Ecuador, Nicaragua, Australia, Papua–New Guinea, Indonesia, British Solomon Is. Ceased commercial operation in 1973.
Aeroservice Corp.	Goodyear AN/APQ-102 (G.E.M.S.)	synthetic aperture	X; 3 cm	HH	37	15	15	Caravelle	*ca.* 12×10^6 km² over North America, all Brazil (RADAM), southern Venezuela. (Amazonas), Colombia (PRORADAM), southern Peru, U.K., several areas of southeast Asia incl. Japan, Taiwan, Philippines; Gabon.
MARS Inc.	AN/APS-94 D Dual-look	synthetic aperture	X; 2.5 cm	HH	100	116	30	Grumman Gulf Stream	*ca.* 3.5×10^6 km² over North America, Central America, parts of southeast Asia, U.K., several countries of tropical Africa incl. Togo, Equatorial Guinea, Nigeria (NIRAD). Aircraft and ownership recently changed.
Intertech Ltd. (for C.C.R.S.)	Willow Run ERIM; now SAR-580	synthetic aperture	simultaneous X (3 cm) & L (23 cm); experimental C (10 cm)	HH normally HV & H & V	5 5 18	1.5 (X) 3 (L) 10	2 (X) 5 (L) 10	Convair 580	*ca.* 750,000 km² over North America, especially Canada and Arctic, Europe.

Martin-Kaye *et al.* 1980) or southeast Asia (see, for example, Froidevaux 1980), relatively little has been published.

Seasat, SIR-A and the European SAR 580 campaign (figure 2*a*) reflect and have encouraged recent interest in radar, which manifests itself in the increasing number and variety of radar papers in remote sensing journals and symposia. The 1981 and 1982 International Geoscience and Remote Sensing Symposia of the I.E.E.E. (Keydel *et al.* 1982), the Snowmass Workshop (Harrison 1980) and E.S.A./EARSeL Workshop proceedings (Guyenne & Lévy 1981) produced particularly significant contributions.

The application of imaging radar specifically to regional resource surveys has been discussed in a general way by Martin-Kaye (1973, 1980).

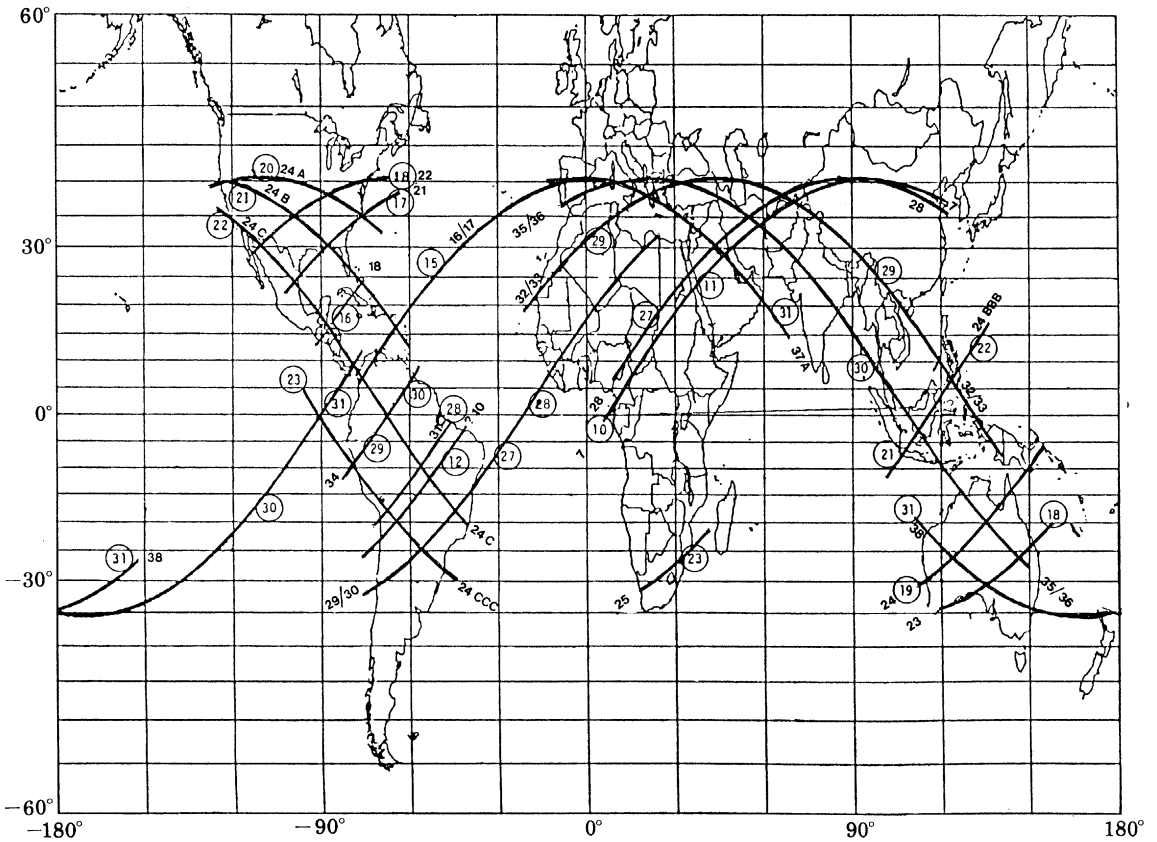

FIGURE 1. SIR-A coverage: circled numbers are reference numbers of orbits; uncircled numbers are reference numbers of SIR-A data-takes. Map prepared by N.A.S.A./J.P.L.

3. PLANNING FOR IMAGING RADAR SATELLITES

In 1964, well before the large commercial regional SLAR surveys had been flown, N.A.S.A. commissioned a study of satellite applications for active microwave systems. It was almost immediately concluded that radar had important potential. By the mid-1970s, further examination (Nagler & McCandless 1975; McCandless & Miller 1975; Matthews 1975, 1978; Rouse 1977), decided upon the launch of an oceanographic radar satellite. This became Seasat-A, put into orbit in 1978.

The need for improved ocean environmental monitoring was, and remains, quite clear, for

such purposes as weather forecasting, hazard warning, ice surveillance and detection of pollution.

The potential of satellite radar also interested the European Space Research Organisation (E.S.R.O.), now the European Space Agency (E.S.A.), which commissioned feasibility studies for a European Sarsat in the early 1970s (Noel & Pelleau 1973).

The E.S.R.O. studies established that there were good arguments for the satellite radar monitoring of dynamic events, particularly for Europe, owing to frequent and widespread cloud cover. The interest has been continued by the E.S.A., which plans an oceanographic radar satellite ERS-1 for the late 1980s (Honvault 1981).

4. Seasat

Seasat was launched from Vandenberg Air Force Base, California, on 26 June 1978. After 1503 revolutions, on 10 October (in U.K.), the system failed and could not be reactivated.

Details of Seasat's operation and application are found in McDonough & Deane (1979), Ford *et al.* (1980), E.S.A. (1981), Sabins *et al.* (1982) and McDonough *et al.* (1983).

Reviews of spaceborne imaging radars including Seasat are given by Elachi (1980) and the National Academy of Sciences (1977).

The principal sensor of Seasat was an L-band, (23 cm) SAR, the data from which were telemetered in real time to the ground. There was no provision for on-board recording, and data recovery was controlled by the location of receiving stations. This limited the coverage to the North American and European regions (table 2).

The total SAR data collected (approximately 20×10^6 Mbits) corresponded to about 2500 min of operation, equivalent to approximately 10^8 km^2 of ground coverage of the radar imagery. An engineering performance evaluation (Held *et al.* 1982; Curlander 1982) concluded that resolution to 6 m $\times$ 21 m, position location to 200 m and relative calibration of image data within ± 2 dB are achievable with the Seasat data set.

The data were either optically or digitally correlated to images, the former being a fairly rapid and elegant process, the latter gaining access to all the data but presenting a large computing requirement.

Data from 53 passes over the European area were recovered by the Royal Aircraft Establishment's receiving station at Oakhanger. The 272 min of recording made by the R.A.E. represents a ground coverage of about 11×10^6 km^2. The image swaths 100 km wide range southward from Greenland to northern Africa; Iceland and the United Kingdom received almost complete coverage but elsewhere there are gaps between the image strips.

Despite the premature failure the Seasat mission had major successes. The SAR was the first such instrument to provide synoptic high-resolution radar images of the Earth's surface. Although the mission was not directed at land purposes overland, imagery was awaited with keen interest. Ford *et al.* (1980) give a review of results in which images are allowed to speak for themselves; some are placed for comparison alongside Landsat MSS, and, in one case, an RBV scene. European, particularly United Kingdom, overland results have been documented for the Royal Aircraft Establishment (Hunting Geology and Geophysics Ltd 1981), in a detailed but limited-edition report that may be inspected at the National Centre for Remote Sensing at Farnborough. An example of Seasat mosaicing and interpretation is given in figure 3, plate 2, and figure 4.

TABLE 2. SPECIFICATION OF MAIN ELEMENTS OF N.A.S.A.S SEASAT SYSTEM

active period	launched 26 June 1978; failure of power system on 10 October 1978 (expected lifetime was one year)
average orbital altitude	790.17 km ± 50 m; period 100.75 min; 14.3 orbits per day; orbit repeat 152 days; nearly circular, non-Sun-synchronous
orbit inclination	nominally 108°; range 104°–108°
total data acquisition time	60 min/day; direct readout to receiving station total 2500 min
coverage	approximately equivalent to 10^8 km², between 72° N and 72° S: North and Central America, Iceland, Europe and north Africa; the United Kingdom's receiving station operated by the Royal Aircraft Establishment at Oakhanger Hampshire, acquired *ca.* 11×10^6 km² over Europe between 1 August 1978 and 10 October 1978 (53 passes, 272 mins total recording time)
alignment	sensor aligned to within 0.07°; pointing angle to within 0.035°; unobstructed view of the Earth
image swath on ground	100 km
image resolution on ground	about 25 m × 25 m (about 40 m for rapid optical correlation, about 25 m × 25 m for precision optical correlation and 6 m × 21 m for digitally correlated imagery)
number of looks	depended on processor; four in most cases
antenna size	10.74 m × 2.16 m fixed
frequency of transmitted signal	1.275 GHz
wavelength of transmitted signal	L-band; 23.5 m
bandwidth of transmitted signal	19 MHz
polarization of transmitted signal	HH
depression angle of transmitted signal	70°
incidence angle at surface of ground	23° ± 3° across swath, from vertical (normal to surface)
peak power transmitted	1000 W
transmitted pulse length	33.4 μs
pulse repetition rate	1463–1640 s^{-1}
time–bandwidth product	634
data recorder bit rate (on ground)	110 Mbit s^{-1} (5 bits per word)
range scale factor	nominally 1:690000 for optical correlated imagery
scale range	± 3%
attributable costs	$400M; launched by Atlas-F rocket
accompanying experiments	radar altimeter, radar scatterometer, visible/infra-red radiometer scanning multi-frequency microwave radiometer (SMMR) similar to that on Nimbus G. Two tape recorders for non-SAR data sufficient to store data from two orbits at 25 kbit s^{-1}
ground stations (all real-time reception for SAR)	Fairbanks, Alaska; Goldstone, California; Merrit I., Florida (all N.A.S.A.); Shoe Cove, Newfoundland (C.C.R.S.); Oakhanger, United Kingdom (R.A.E.); Canary I. (both E.S.A.)

DESCRIPTION OF PLATE 1

FIGURE 2. (*a*) Comparison of SLAR bands X (3 cm) and L (23 cm), Buxton, U.K., SAR 580. Optical correlated imagery. Scale approximately 1:100000. Resolution is 1.5 m × 2.1 m for X-band and 3 m × 5 m for L-band. The mesa-like hill is formed from mid-Carboniferous gritstone more or less horizontally bedded and covered by a thin blanket of hill peat and moorland low scrub. Buxton, dry-stone walls, roads, trees, quarries are well represented on both X and L images, although X-band better delineates individual radar reflectors. The generalization of features on L-band can help rapid recognition of features, e.g. stands of trees, the outline of Buxton.

(*b*) Seasat image of mountains and glaciers in Greenland. The direction of look is from the top of the image; 'chevrons' and conspicuous layover (see particularly the layover of the mountain peaks adjacent to the glaciers) are produced by the steep depression angle of Seasat.

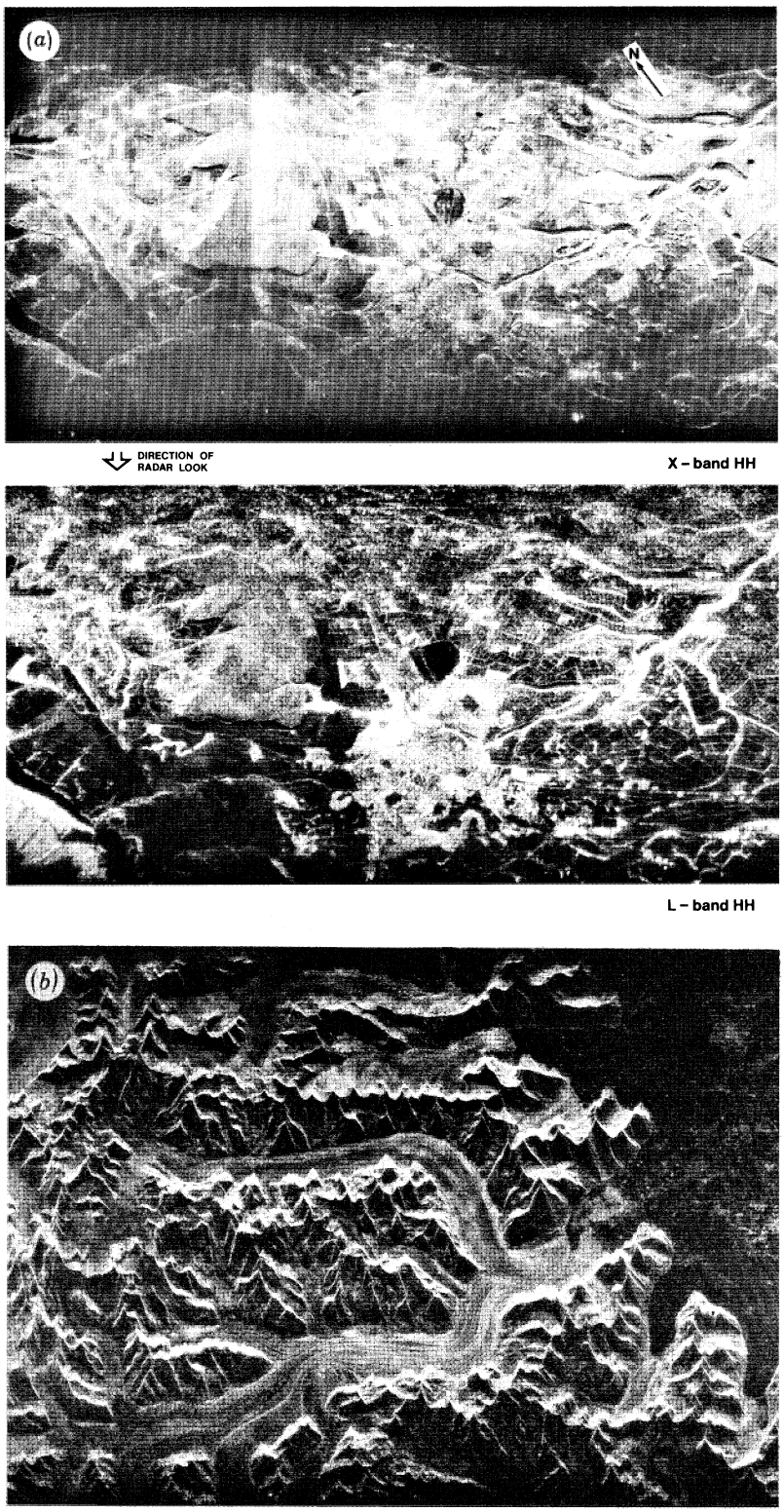

FIGURE 2. For description see opposite.

(*Facing p.* 300)

FIGURE 3. Seasat radar mosaic of the United Kingdom and adjacent Ireland, constructed by Hunting Surveys Limited for the R.A.E./E.S.A.-Earthnet and N.E.R.C. (N.A.S.A.'s Seasat 1 SAR data acquired at R.A.E. Oakhanger and optically correlated by E.R.I.M., U.S.A.).

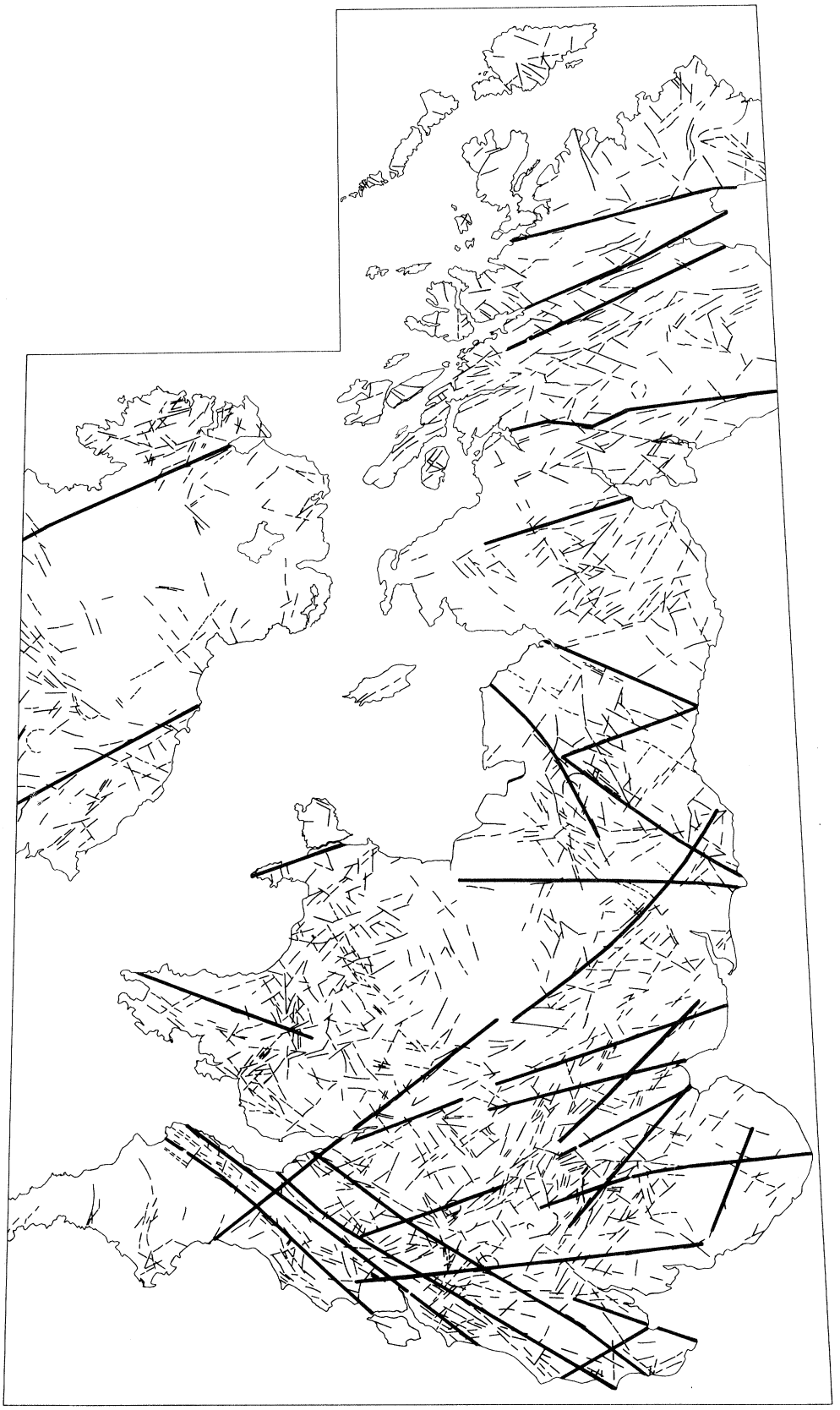

FIGURE 4. Rapid preliminary interpretation of geological lineaments of Seasat mosaic of United Kingdom.

The Seasat SAR configuration was for oceanographic work and was not fully appropriate over land. The large depression angle led to severe foreshortening and layover effects (figure 2*b*, plate 1). In mountainous country these effects prevented any but the most generalized interpretations. However, for areas of modest relief and flatland the data were amenable to interpretation at regional to semi-detailed scales (i.e. 1:100000 to 1:500000 scale for geological and 1:50000 to 1:100000 scale for land-use purposes). The level of interpretability relates to the mode of processing, improving from 'survey mode' material, which is rapidly processed, optically correlated imagery (bulk processing), to precision optically correlated imagery and to digitally correlated imagery (table 2).

Major physiographic units (land and sea, mountain ranges, plateaux, coastal and inland plains, etc.) and the general nature of the landscape (e.g. flat, rolling, irregular, hummocky, mountainous; forested, arid, cultivated, swampy), are well differentiated on Seasat imagery. Geological structures (major lineaments, faults and folds) are sometimes expressed very distinctly (figures 3 and 4). Lines of trees, woodland areas over 5 ha, and heathland and moorland over 50 ha are readily identifiable. Man-made constructions of 100 m or so and more and in sufficient contrast to the surrounds (e.g. airport runways, embankments, long piers, major bridges, canals or large isolated buildings) can be seen.

Less clearly differentiable, or variably so, are lakes, intermediate drainage, lowland coastlines, towns and villages, pasture, meadow and parkland. Where solid geology is masked by any form of cover (e.g. soil, vegetation or urbanization), lithologies can only be inferred from morphology, which may be uninformative. Lesser roads usually cannot be seen; even railways often cannot be distinguished although some are conspicuous. (See also figure 2*a*, comparing L-band with X-band radar.)

Interactive computer processing of digital Seasat data brought little improvement of interpretability. The data were monospectral, and the number of processing options is hence limited. There was more benefit for land-use mapwork than for geology, at least in temperate European circumstances.

5. Landsat and Seasat

The information level in data from the MSS of Landsats 1, 2 and 3 is mostly greater than from Seasat SAR (Pala *et al.* 1980), despite the better resolution of Seasat. This is certainly true for areas of high mountain relief because of distortions due to radar ranging, but is also generally so elsewhere. Sometimes, as shown in some of the illustrations of Ford *et al.* (1980), there is more detail obtainable from Seasat. Over ice, lava, drumlin fields, braided drainages, meander flats and variable deserts (hamadas or sand seas), differentiation may be better, and the same applies in particular circumstances for many other features. Owing to radar's sensitivity to slope, geological structures expressed only subtly by relief may be seen better on radar imagery.

On account of the distortions in side-looking radar imagery, complete registration between Landsat and Seasat images can only be approached for flatland conditions. Numbers of such digital composites have now been reported upon (see particularly the co-registrations of Elachi *et al.* (1982*a*), Ford (1982) and Blom & Daily (1982)). The procedure involves the resampling of Seasat digital data to compatible pixel size and to Landsat swath orientation. The two data sets have individual contributions that are mostly best considered alongside each other rather than in combination.

Digital superimposition of data from different Seasat SAR overpasses to compare multitemporal

information is readily achieved. Locations and areas of change may be speedily discriminated by colour-coding the two outputs appropriately, as for example in Martin-Kaye *et al.* (1983).

The evaluation of Seasat overland led to several clear conclusions. In the European context, the distribution of the majority of topographic, cultural and geological features of the continent is well known. There is no need to resort to radar satellites to establish their existence or whereabouts, although interesting new perspectives can be obtained from space and the synoptic views. Seasat did yield new geological information in the depiction of unsuspected linear features in the relative flatlands of southern England and doubtless could do the same elsewhere (figure 4). So far as can be seen, it is not necessary to inspect these with systematic regularity, although images from different seasons might provide some complementary information. Purposes of this nature do not make a convincing case for an unmanned radar satellite over European land areas. The value would mainly lie in crop inventory and the monitoring of crop state, leading to improved crop yield forecasting, a purpose that SAR has some capacity to satisfy.

6. Shuttle imaging radar: SIR-A

(*a*) *The system*

SIR-A, the Shuttle imaging radar, was one of the seven experiments of the first scientific payload of the Space Shuttle Columbia, carried on the second flight launched on 12 November 1981 (table 3). The payload concerned remote sensing of land resources, environmental quality, ocean conditions and meteorological phenomena (figures 5 and 6). The flight was curtailed, causing abandonment of the original SIR-A coverage plan. Nevertheless, the full 8 h capacity of the on-board optical film recorder was used and about 10^7 km^2 was imaged. The on-board recording freed the enterprise from the tether of ground receiving stations, which limited Seasat. SIR-A swaths spanned continents and oceans between about 40° N and 40° S latitudes, greatly extending the variety of geographic coverage and of terrain types inspected by mapping radars (figure 1). The experiment was a notable success in geological application, to which it was primarily directed, particularly in the demonstration of the extent of radar's capacity for lithology-related discriminations in bare rock areas, its sensitivity to subtle, possibly buried, features in dry desert sands, and its sensitivity to moisture in bare soils.

The radar was of Seasat type, also operating in the L-band (23 cm). There were important differences in configuration and the philosophy of the experiment. An operational monitoring role suits the repetitional global-ranging performance of non-geostationary satellites. The single-mission capacity and flexibility of the Shuttle lend it to experiment and once-only or occasional inventories. Columbia was launched with the SIR-A antenna fully deployed in the cargo bay (figure 5), thus ensuring an integrity not easily equalled in unfolding structures. For the geological objectives the critical difference in the system between Seasat and SIR-A was the smaller depression angle of SIR-A (table 3).

(*b*) *Preliminary results and general comment*

Only a few of the first results of SIR-A studies have yet been published. The first preliminary accounts of SIR-A have been given by Elachi *et al.* (1982*b*), Elachi (1982), Covault (1982), Taranik (1982), Estes (1982), Kobrick (1982) and Hubbard (1982). The present comments are based upon those sources and studies in progress in the U.K. Most of the non-U.S. coverage by SIR-A is held in the United Kingdom by official observers to the experiment.

SIR-A imagery is impressive. Detailed examination shows that, geologically, it is interpretationally satisfactory at the delivery scale (nominally 1:500000) and for some areas carries significant new information. Detail can be excellent (figure 7, plate 3).

TABLE 3. SPECIFICATIONS OF MAIN ELEMENTS OF SHUTTLE IMAGING RADAR (SIR-A) SYSTEM

(Optical recording only.)

active period of Shuttle	launched 12 November 1981; returned 14 November 1981: 54 h
average orbital altitude of Shuttle	circular; 257–266 km (av. 137 naut. miles)
orbit inclination	38°
total data acquisition time	8 h
coverage	see figure 1; parts of 60 countries between 40° N and 40° S
area covered	*ca.* 10^7 km^2; *ca.* 6×10^6 km^2 over land
image swath on ground	50–55 km
image resolution on ground	40 m × 40 m
number of looks	4–7 (4 or 5 in practice)
antenna size	fixed, 2.1 m × 9.35 m
frequency of transmitted signal	1.3 GHz
wavelength of transmitted signal	synthetic aperture; 23.5 cm (L-band)
bandwidth of transmitted signal	6 MHz (optical recorder)
polarization of transmitted signal	HH
depression angle of transmitted signal	43° at centre of swath
variation of depression angle across swath	± 3° from centre
incidence angle at surface of ground	50° ± 3° from vertical
peak power transmitted	1000 W
range scale factor (slant range imagery)	nominally 1:500000
scale range	1:485000 to 1:515000
signal film type	3650 ft Kodak RAR 3493, 70 mm wide
film speed	nominally 37 mm s^{-1}
range focal length	300 mm
azimuth focal length	2 m
range spatial frequency range	3–34 mm^{-1}
azimuth spatial frequency maximum	44 mm^{-1}
designed surface backscatter cross section response	−8 to −28 dB
attributable cost, OSTA-1: $11.6M plus $4.4M integration	
attributable cost, SIR-A: $9M	
accompanying experiments:	ocean colour experiment scanner (OCE), scanning microwave infrared radiometer (SMIRR), FILE, MAPS (figure 3)

Speckle is quite pronounced in the bulk-processed images currently available. At the delivery scale it is not obtrusive but enlargement beyond 1:200000 scale renders it conspicuous (figure 12, plate 8).

High mountain relief produces the usual distortions resultant from radar ranging, but the effects are notably less severe than for Seasat, where the depression angle was larger (figure 16, plate 12).

(*c*) *Results over tropical regions*

Some tropical forested areas were imaged from space for the first time by SIR-A. The cloud cover of the Pakaraima Mountains, Guyana (figure 14*a*, *b*, plate 10), for example, has resisted the endeavours of Landsat since 1972. In such regions geological interpretation is essentially based upon morphology. However, because of the good depiction of morphology by radar shadowing, some areas are remarkable for the geological data content in spite of the forest cover. The Rio Uaiauka area of southern Venezuela (figure 13, plate 9) is a particularly good example. More subtly expressed information from tropical rainforest is shown in figure 14*e*.

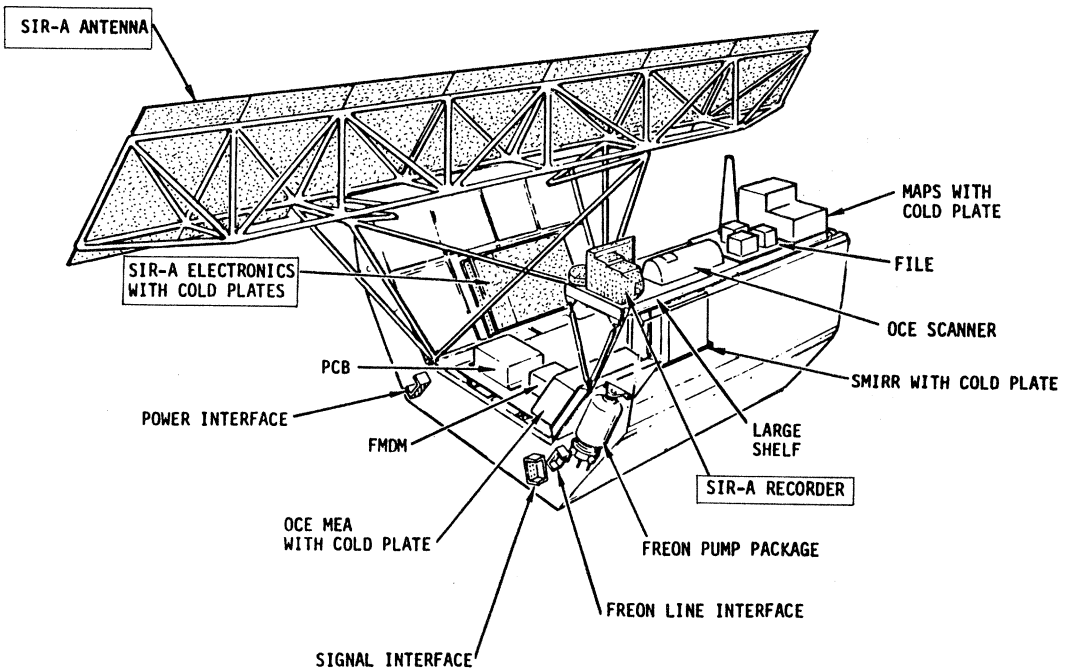

FIGURE 5. OSTA-1 pallet on board the second Shuttle flight, November 1981, showing SIR-A equipment. (After Taranik (1982).)

New information is carried in the detail of these illustrated examples of tropical rainforested regions. Systematic global coverage at this level of quality would be an enormously important baseline data set. An example of an instant application is given in figure 14*c*, *d*, which shows part of the Gran Sabana of Venezuela, near to the Guyana border. Strong lineaments converge on circular features that seem hitherto to have been unrecorded. They may mark intrusive bodies that have escaped notice among outcrops of the large basic sills interspersed in the quartzites and conglomerates of the Roraima Formation. An attractive speculation is that they are diamond-bearing pipes, the source of the diamonds distributed about the Roraima plateaux; this source is at present unknown. Structural information of immediate use in hydrocarbon prospecting can be seen in the example from West Irian (figure 14*f*) (see for comparison Froidevaux (1980)).

(*d*) *Results over arid regions*

SIR-A produced a surprise in the unexpected diversity and detail of geological information from arid areas.

Dry sands, even some dunes, show little radar feature if without vegetation (Blom *et al.* 1982); they appear as dark image tones representing low or no backscatter (figure 10, plate 6; figure 15*c*, *d*, plate 11). Drainage courses are well depicted where fine dry sand fills the channels (figure 8, plate 4; figure 9*b*, plate 5). This precise delineation of drainage and clear depiction of sand sheets suggests that spaceborne imaging radar can have an important role to play in desertification and hydrogeological studies.

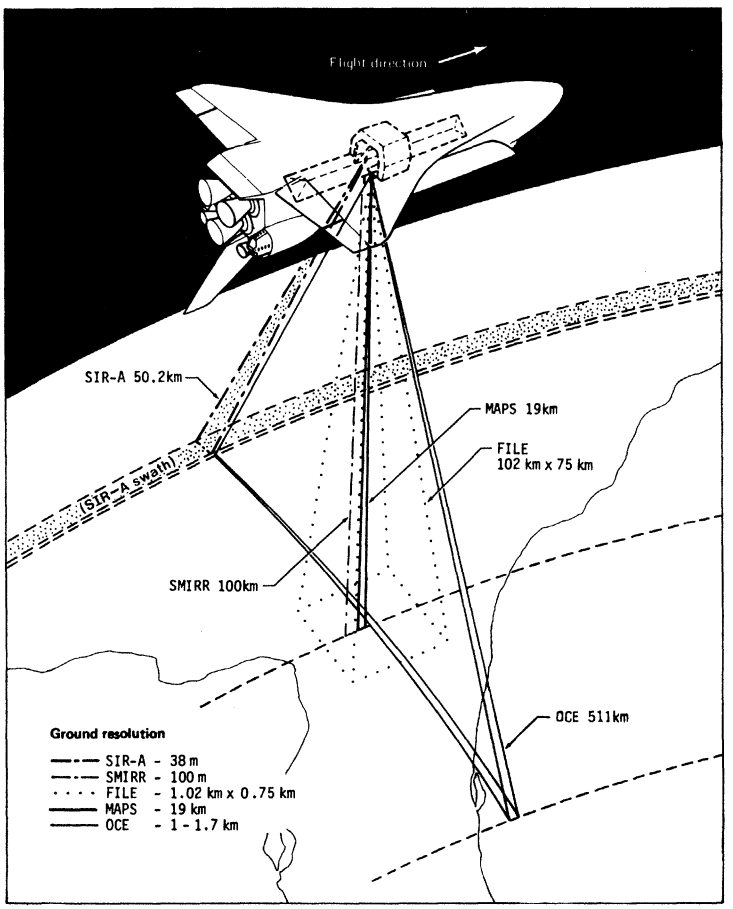

FIGURE 6. OSTA-1 experiments on board the second Shuttle flight, November 1981, showing SIR-A swath. SMIRR, Shuttle multispectral infrared radiometer (a non-imaging experiment to determine the most suitable i.r. bands for lithology recognition); FILE, feature identification and location experiment (uses ratio of visual red and near-infrared reflectance for data management purposes); MAPS, measurement of air pollution from satellite (determines CO in the troposphere); OCE, ocean colour experiment (measures blue-green colour variation via scanner). (After Taranik (1982).)

The absence of vegetation can lead to images in which geological structure is spectacularly displayed (figures 10, 11 and 15*a–c*). The presence of evaporites may complicate the interpretation as in the Grand Kavir salt desert of Iran (figure 15*a*). Salt plugs provoke a variable but distinct speckly bright to grey tone of distinctive context (see also Carver & Bush 1979).

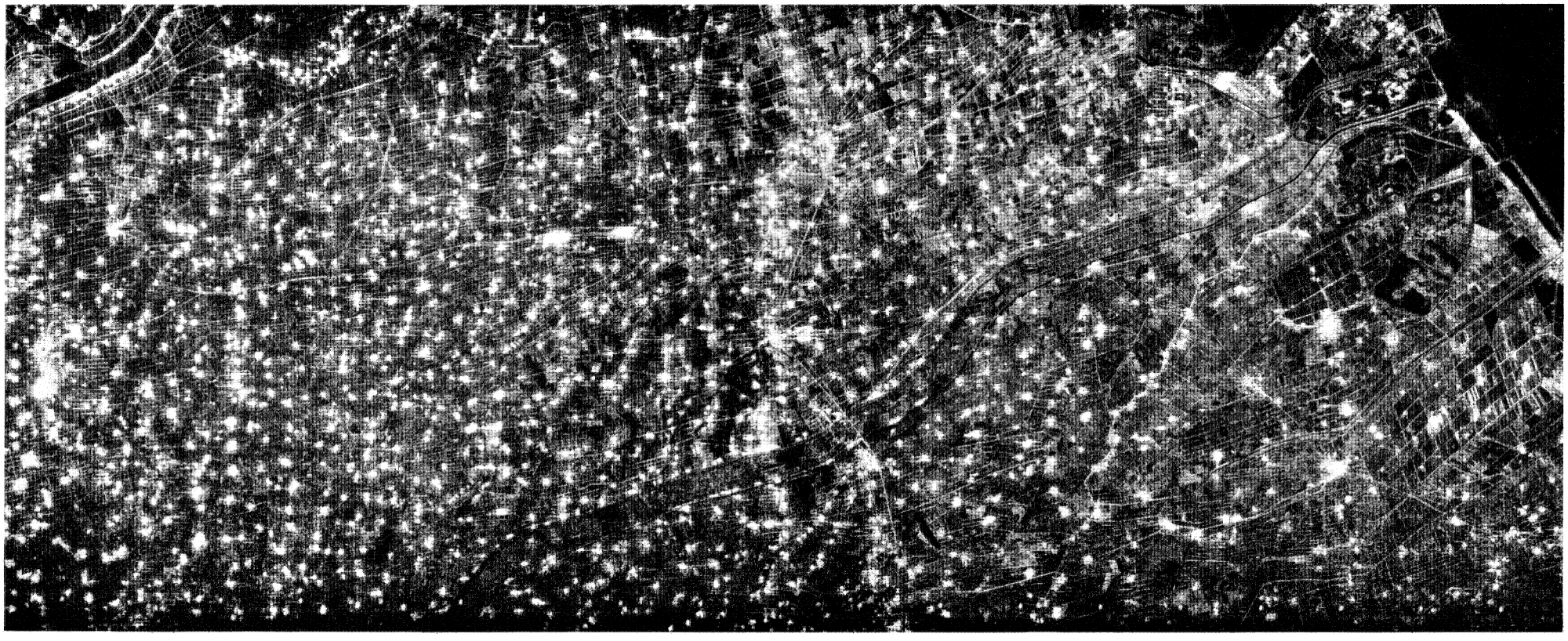

FIGURE 7. SIR-A image (data-take 7) over densely populated and cultivated alluvial/loess plain of north China, near Peking. Nominal scale 1:500000. The bright reflectors are towns and villages. Roads and tracks show clearly from the black tones of flat waterlogged fields. North is to bottom of image.

(*Facing p.* 306)

FIGURE 8. SIR-A swath 29/30 over Adrar des Iforas, northeast Mali. Scale nominally 1:500 000. Bright areas are rough-surfaced outcropping rock; black tonal areas are thick sand. 'Younger Granite' ring-intrusions and associated dyke-swarms and the Iforas granulite unit are particularly distinct. The radar illumination is from top of image, north is to bottom left corner. The area of the subscene in figure 9*b* is shown. The margins are not rectangular because the subscene has been 'warped', on an image processor, to co-register with Landsat.

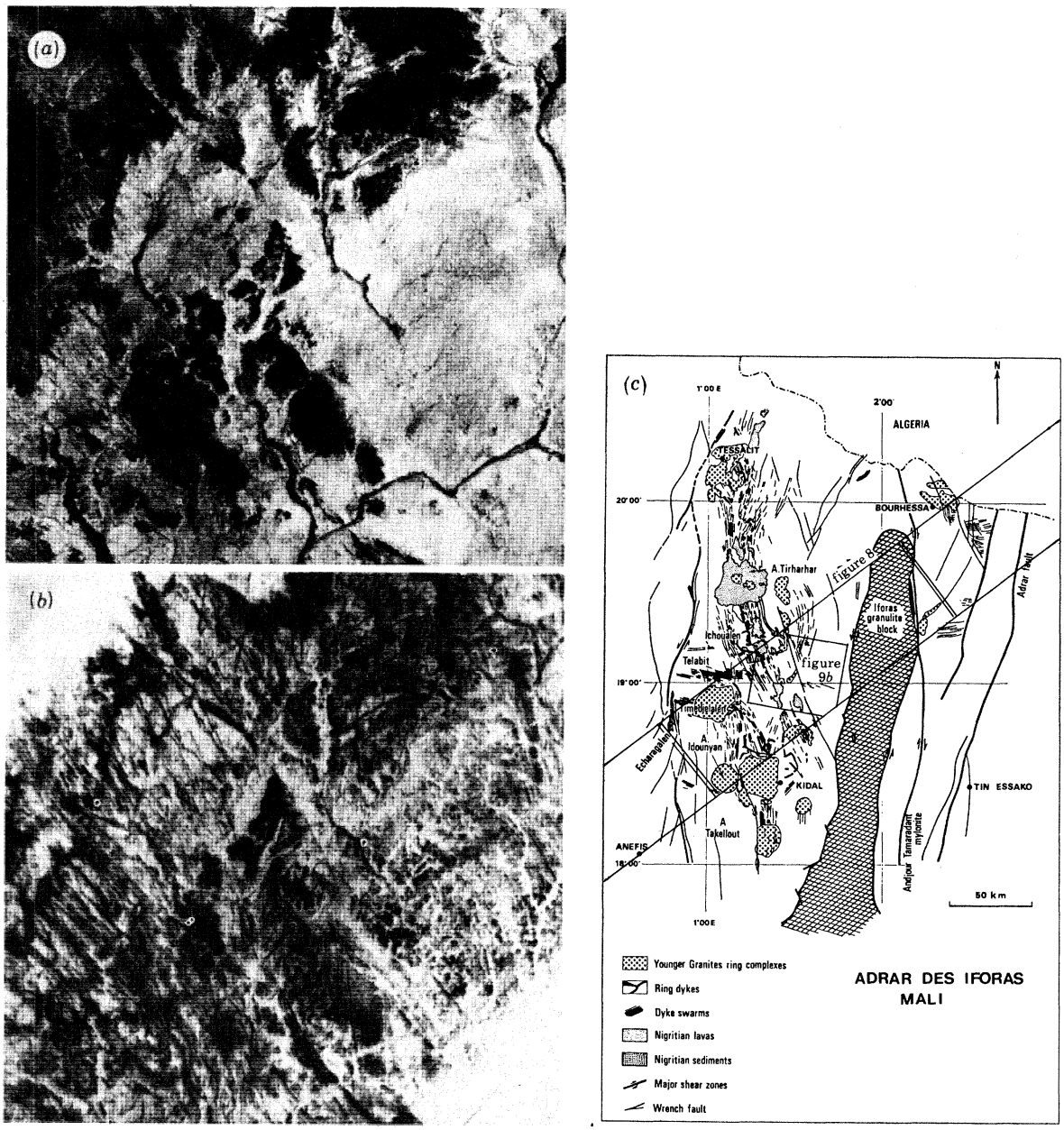

FIGURE 9. (*a*) Adrar des Iforas; Mali Landsat MSS subscene enhanced and warped to co-register with SIR A image on Hunting's image processor (reproduced in monochrome).

(*b*) Equivalent SIR-A image reproduced as negative (bright radar tones reversed to appear black). The bright-reflecting low-relief sand/gravel areas of the Landsat compare with minor drainages and outcrop and perhaps sub-outcrop on the SIR-A (especially the bottom right corner). The dyke swarm shows much more clearly on the SIR-A and a possible small circular feature is identified within a larger circular (top left). The SIR-A imagery responds to small outcrop and boulders better, resulting in more detail, than Landsat because of the former's better resolution (40 m × 40 m compared with 50 m × 80 m for Landsat) and its response to surface roughness. In this very dry area there is also possible shallow penetration and backscatter return of the SIR-A radar beam from subsurface bedrock.

(*c*) Geological sketch of Adrar des Iforas, northeast Mali, showing SIR-A swath (data-take 29/30) and subscenes of figures 8 and 9*b*. (After Black *et al.* (1979).)

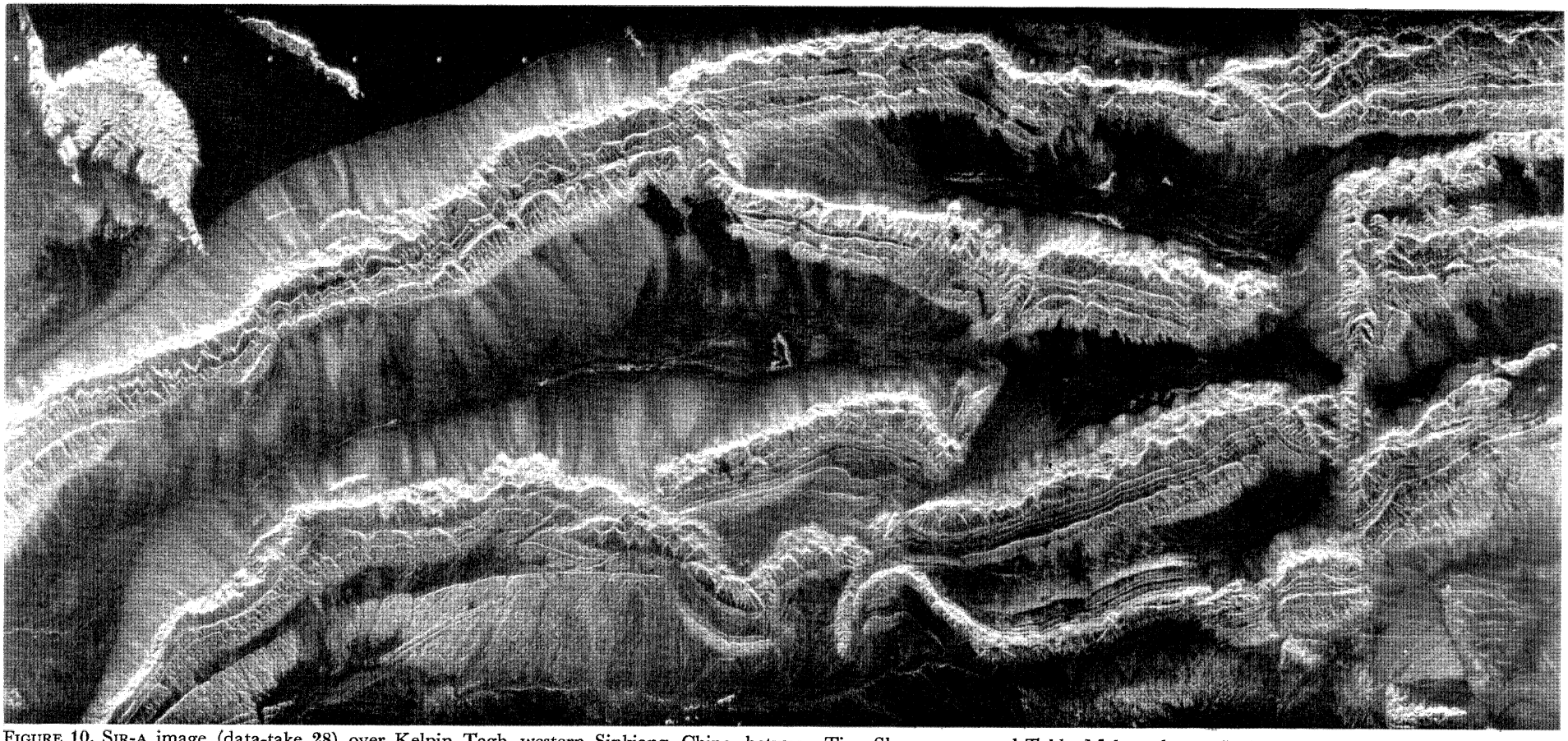

FIGURE 10. SIR-A image (data-take 28) over Kelpin Tagh, western Sinkiang, China, between Tien Shan ranges and Takla Makan desert. Scale approximately 1:500 000. In this arid area folded and thrusted sedimentary rocks are cut by prominent transcurrent faults. Thrust planes dip northward (towards bottom of image). Large cuestas are surrounded by alluvial fans whose rough cobble and boulder surfaces provoke a bright radar response. The boundary between fans and desert sands, which have almost no radar backscatter, is distinct (top left of image). Radar illumination from top of image at approximately 50° incidence angle; north is approximately to bottom left of image. The white dots are fiducial marks representing each second of the Shuttle's orbit.

FIGURE 11. Landsat MSS band 7 image over Kelpin Tagh, western Sinkiang, China. Landsat path/row 159/32, 15 May 1973, centre point N 40° 25′, E 78° 17′. Sun elevation 59° from southeast (top left-hand corner). The better resolution and depiction of surface roughness of the SIR-A results in better definition compared with Landsat.

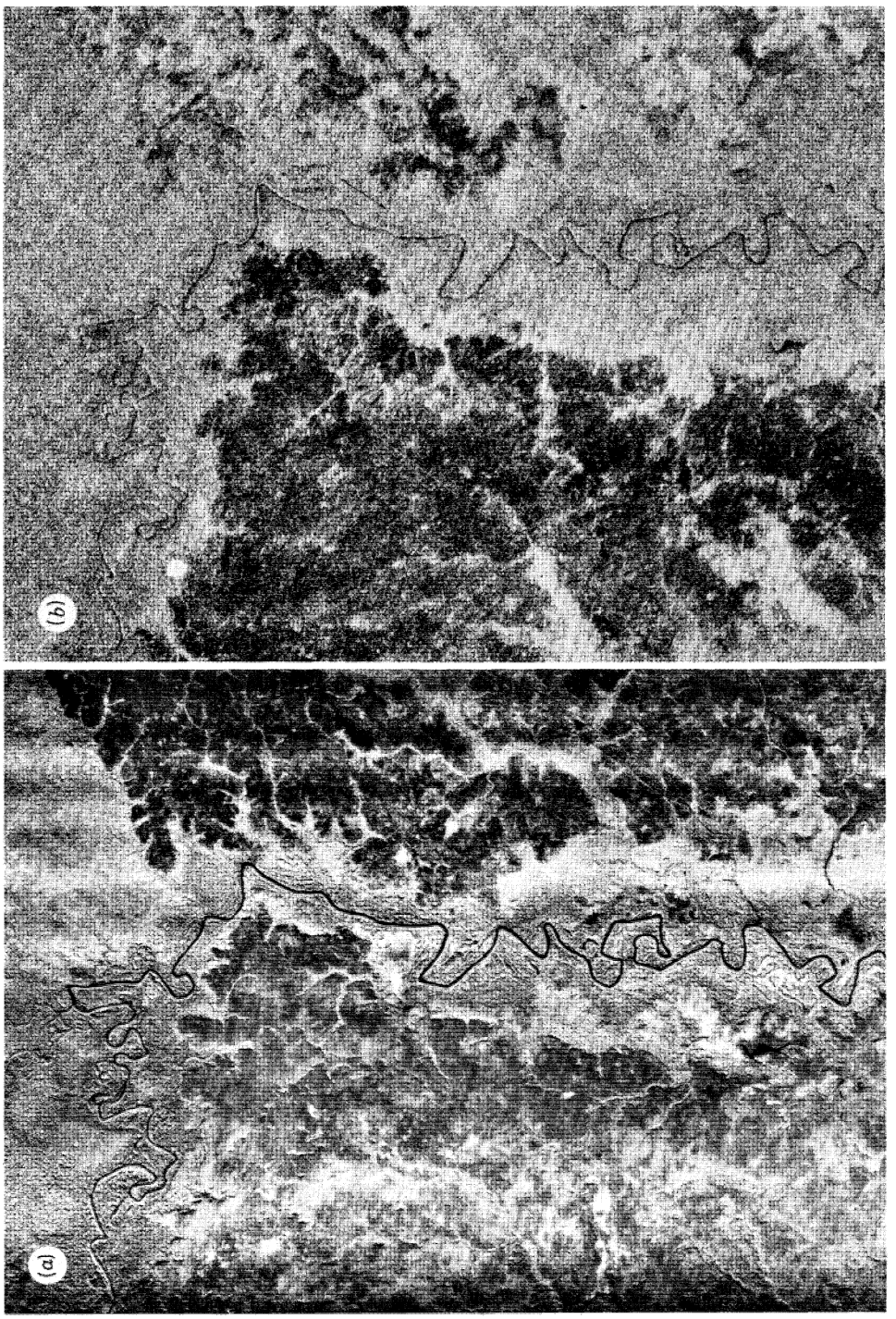

FIGURE 12. For description see opposite.

Description of plate 8

Figure 12. Comparison of (*a*) Westinghouse Ka (0.86 cm) SLAR and (*b*) L-band (23 cm), SIR-A (data-take 24C) over low-relief area of northeast Nicaragua. Scale nominally 1:200000. Area of forest and cleared forest savanna underlain by clays and gravels. Although the SIR-A has distinctly inferior resolution (40 m compared with 10 m) laterite-surfaced roads can show well. Differences of tone on the imagery are thought to be due to temporal changes (the two images are 10 years apart, but both of wet season) rather than radar wavelength differences. The dark interfluve areas are probably waterlogged savannah. The radar illumination is from the right-hand side of the image for the SLAR, at an incidence angle of *ca.* 60°; that for the SIR-A is from the top left-hand corner of the image at an incidence angle of 50°. Note that the marked difference of radar illumination and depression angle do not materially change the delineation of radar geological units.

Note added in proof 16 (*March* 1983). Radar depression angle is, of course, substantially variable across the SLAR swath (*a*), being larger in near range (right-hand side) and smaller in far range. The depression angle at centre of swath is equivalent to that of SIR-A but from approximately the opposite direction. The cleared-forest grasslands appear darker at the larger depression angle of the near range of SLAR. The SIR-A (*b*) may be showing a similar but smaller effect in the reverse direction; the depression angle variation across swath of SIR-A is only 5–6° compared with the 30–40° of SLAR.

Description of plate 9

Figure 13 (*overleaf*). (*a*) SIR-A image (data-take 34) over part of southern Amazonas, Rio Uaiauka, Venezuela. Nominal scale 1:500000. Inaccessible low-relief area of tropical rain forest underlain by well fractured rocks (left) mapped as acid extrusive rocks set in Lower–Mid-Proterozoic granites and migmatites of the Guiana Shield. The pronounced circular feature is probably a granite ring-intrusion (not shown on maps). The distinct mesa-like form comprises probable Lower Roraima Formation (or an older unit) arenites of ?Mid-Proterozoic age, draped, and possibly gently warped, over the older rocks. Remnants of the tabular arenites on the well fractured Basement rocks account for the preservation of these older rocks. A faulted fold of metasediment or volcanic horizon emerges prominently from featureless Basement rocks (bottom right). Note that the image over this forested area contains no direct radar-signature of lithologies. Context, morphology and inferred geological structure impart, however, substantial indirect information on lithology. The scarp of the Lower Roraima is emphasized by its being perpendicular to the radar signal. The white dots are fiducials representing each second of the Shuttle's flight. Radar illumination is from the top of the image and north is to the bottom left corner.

(*b*) Preliminary geological interpretation of (*a*) at 1:000000 scale. X, Rio Maraca shear zone in Basement. Full key given in the legend to figure 14.

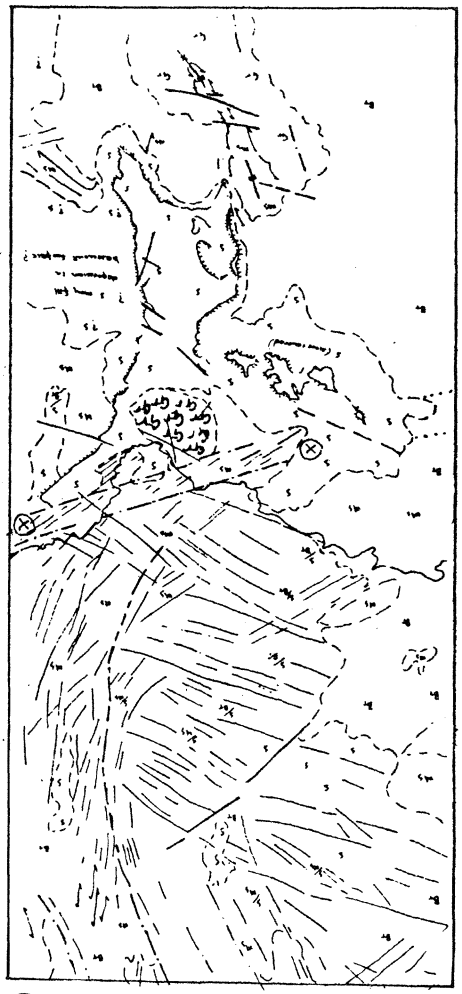

FIGURE 13. For description see previous page.

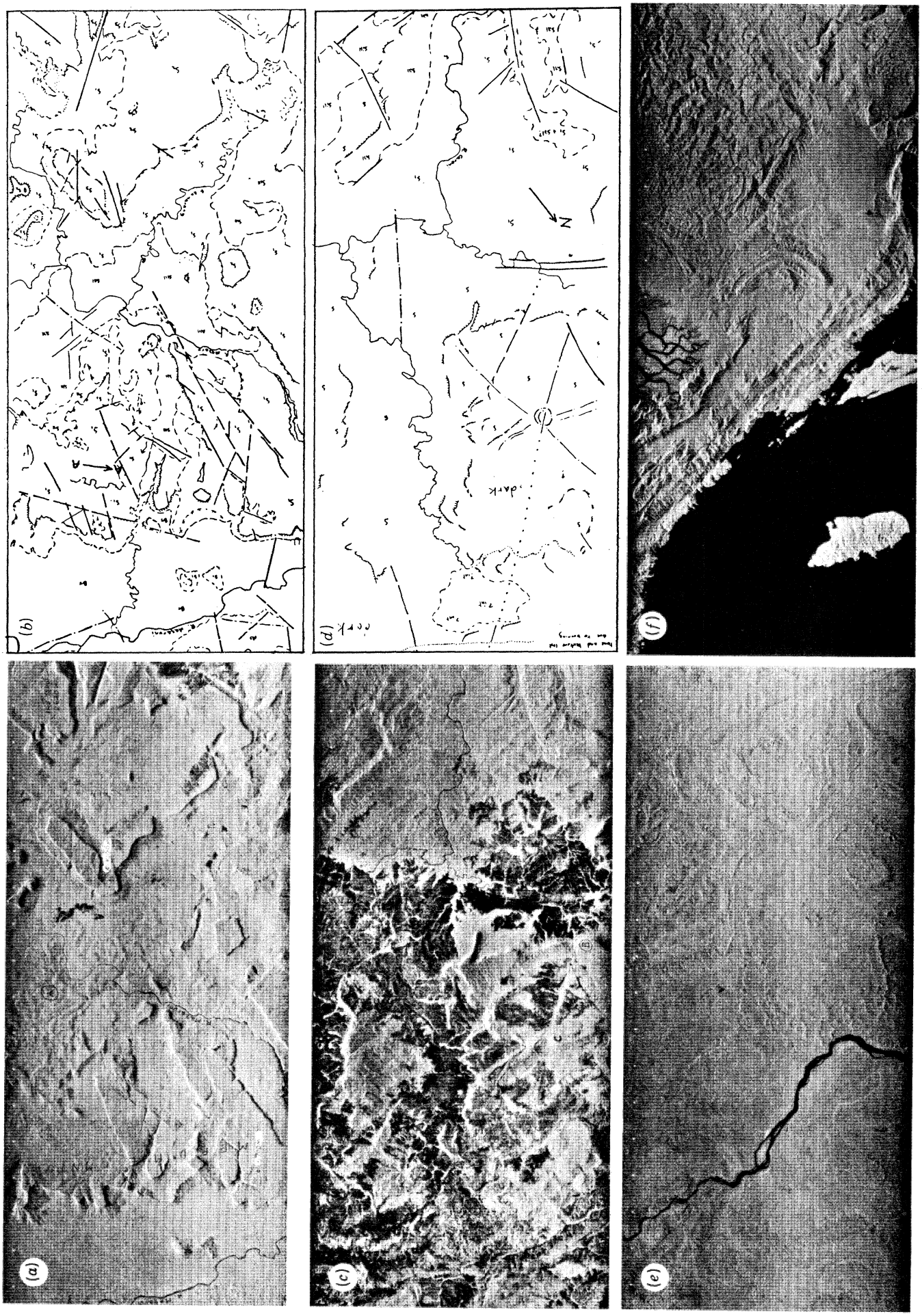

FIGURE 14. For description see overleaf.

Description of plate 10

FIGURE 14. SIR-A over tropical regions at nominal 1:1000000 scale; radar illumination is from approximately southward, i.e. from top of each image.

(*a*, *b*) Western Guyana and eastern Venezuela (data-take 34). Forested Pakaraima Mountains and River Mazaruni Basin. Proterozoic clastic arenites of Roraima Formation form massif slabs with steep scarps; basaltic sills at A and partly waterlogged savannah (dark low relief areas) of La Gran Sabana at B Low ground on left underlain by gneisses of Guiana Shield.

(*c*, *d*) Eastern Venezuela (southeast Bolivar), and La Gran Sabana and Rio Caroni (data-take 34). Dark areas are partly waterlogged upland plateau savannah at 1000–1500 m. Note strong linear fracture A-B-A′ and circular features at C. Alluvial diamonds in the region have not been traced to source and one can speculate that these circular features are traces of kimberlite intrusion.

(*e*) Mid-Amazon Basin, Brazil (data-take 24C). Dense rain forest and subtle traces of ?Carboniferous sediments.

(*f*) Lengguru fold belt, Vogelkop Peninsula, west Irian (data-take 32/33). Folded Tertiary sediments in dense tropical rain forested mountains.

Key to figures 13*b* and 14*b*, *d*. S, sedimentary formations, subscript indicates superposition, S_1 being oldest. Roraima arenaceous formations. Ms, Precambrian metasediments; d, dykes; sill, basaltic sills of Roraima Formation; int, igneous intrusions; Gr, Precambrian granitic plutons; Gns, Precambrian gneiss; BT, deeply weathered 'Basement' migmatites and granites, etc., masked by lateritized soils and vegetation.

Description of plate 11

FIGURE 15. SIR-A over arid regions at nominal 1:1000000 scale; radar illumination is from approximately southward, i.e. from top of each image.

(*a*) Grand Kavir salt desert, north central Iran (data-take 28). Prominent but low-relief faulted anticlinal fold of mid-Tertiary continental sandstones and shales (producing alternate rough and smooth surfaces) apparently pierced by a salt-plug (not shown on geological maps). Surrounding areas are flat-lying Quaternary playas, silt and sand. Conspicuous salt plugs (Neogene) are especially well delineated by the L-band radar (right of image).

(*b*) Western Sahara (data-take 32/33). Remarkable sequence of regularly bedded Devonian arenaceous sediments showing minor faulting and drag-folding.

(*c*) Chaîne d'Ougarta, western Algeria (data-take 32/33). Cores of Upper Proterozoic sediments and volcanics surrounded by Lower Palaeozoic sediments. A dune field shows as a distinct black tone with dune features picked out by moderate backscatter from coarser materials and interdune areas.

(*d*) East of Ndjamena, Chad (data-take 28). Barchan-dune field derived from Lake Chad ancient deposits. Older long linear vegetated dunes can be seen at top right.

(*e*) West Queensland, Australia (data-take 35/36). Braided drainage of the Rivers Diamantina (left) and Hamilton (drains to Lake Eyre), crossing a mostly low-relief arid savannah underlain by Mesozoic platform-cover sediments outcropping at A. The bright tones of the drainage and outcrop results from radar backscatter from rough surfaces, in excess of a few centimetres trough-to-peak 'relief' according to Rayleigh formula. The black tones result from lack of backscatter from flat-lying waterlogged, and sand- and clay-covered, surfaces.

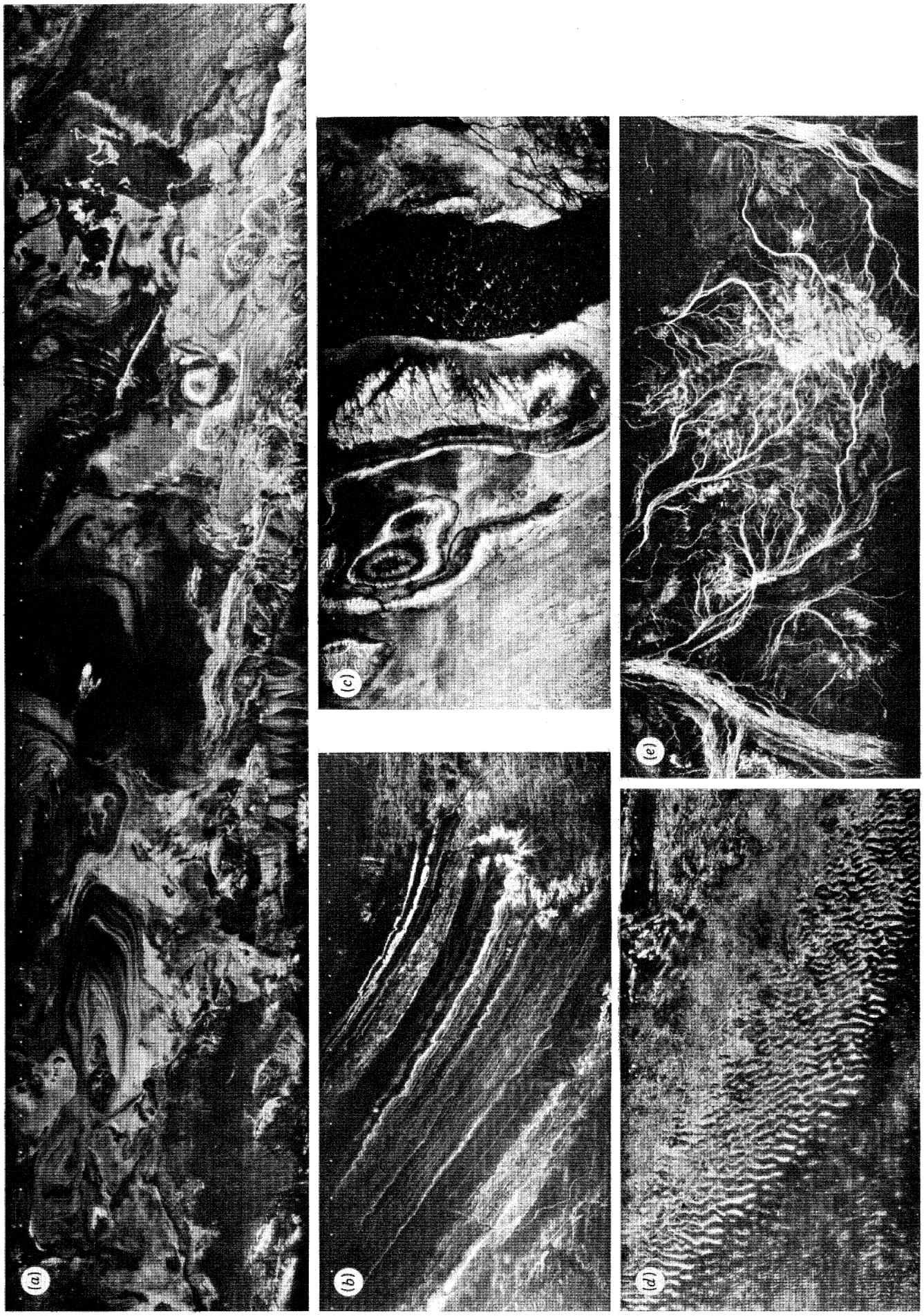

FIGURE 15. For description see opposite.

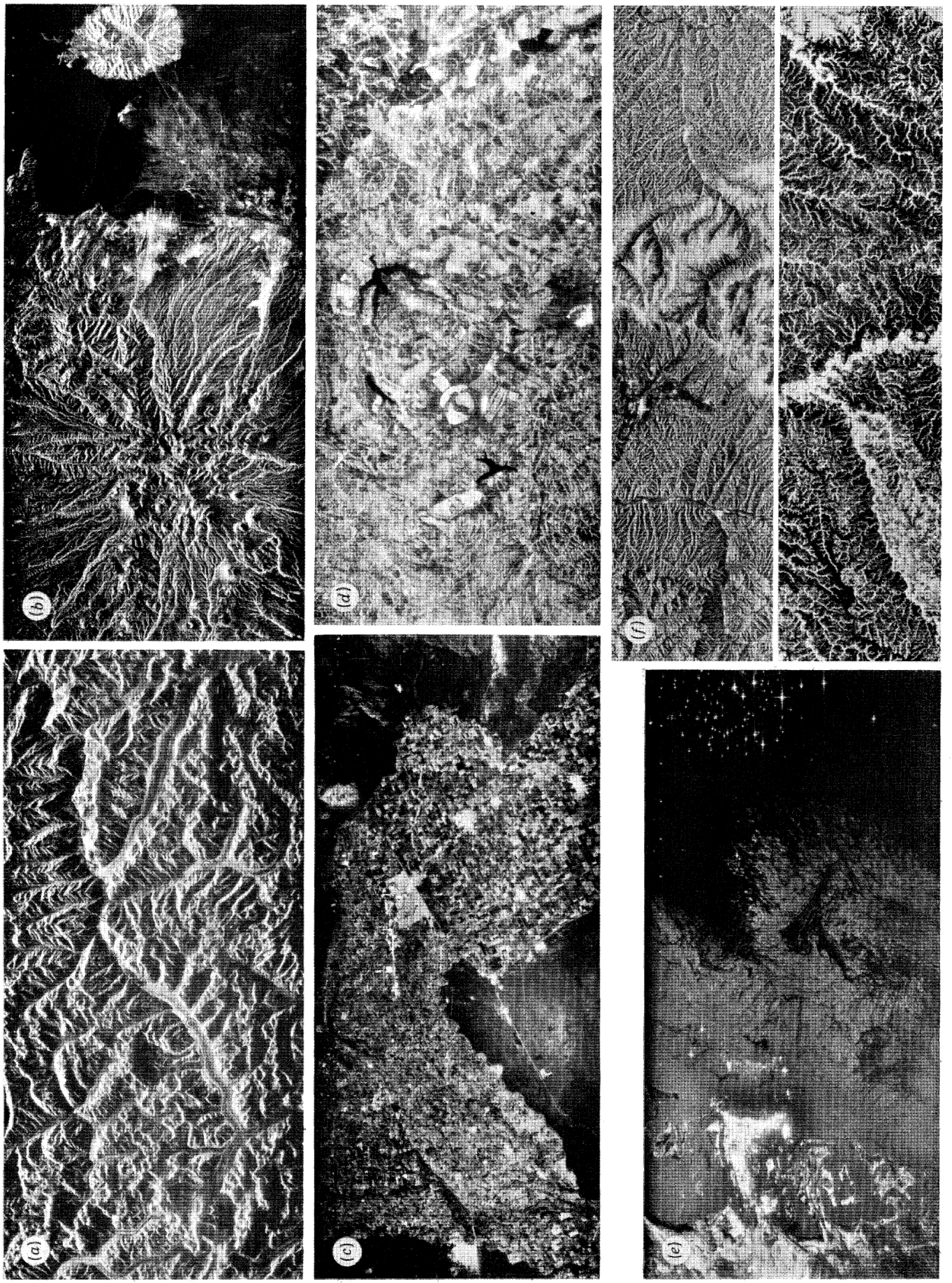

FIGURE 16. For description see opposite.

In low-relief arid regions the roughness of the surface is the predominant control of radar backscatter, as has been previously recognized from smaller areas inspected by SLAR and Seasat (Schaber *et al.* 1976; Daily *et al.* 1978; MacDonald & Waite 1973), and seen over wide areas on SIR-A images (e.g. figures 10 and 15*e*).

In the very arid Adrar des Iforas, northeast Mali, surface roughness is particularly well recorded on SIR-A imagery (figures 8 and 9*a–c*). The Adrar des Iforas forms a southwest extension of the central Saharan Hoggar Shield, and comprises Upper Proterozoic and reworked older basement sliced by major north-trending shears and comprehensively intruded by granitoid intrusives and volcanics. The central shear-bounded Iforas granulite unit (Eburnean age) is well shown on both Landsat and SIR-A (figures 8 and 9). To the west of the granulite unit, late Proterozoic granitic batholiths are intruded by prominent ring-intrusions of alkali granites, rhyolite and associated dyke swarms, which are especially well depicted on the SIR-A image (figure 8).

The Iforas SIR-A image presents substantially more information than the equivalent Landsat image, in part owing to the better resolution of SIR-A (40 m × 40 m compared with 50 m × 80 m of Landsat). There is also a possibility that the SIR-A L-band is penetrating dry surface sands and fine gravel, and backscattering from shallow-buried sub-outcrop (see for example the case of Sudan/Egypt (Eberhart 1982; Elachi *et al.* (1982*b*)). Work in progress in the U.K., however, suggests that this phenomenon may be limited to small areas and that it is the response to surface roughness and the better resolution that result in the greater data content of SIR-A (Lawrence & Martin-Kaye 1983). Examples similar to southern Egypt have been noted for central and northwest Saudi Arabia, central China and elsewhere.

(*e*) *Studies for agriculture, land use and other purposes*

The SIR-A experiment was designed for geological purposes and no systematic land-use studies have yet been reported. The resolution of the bulk-processed material, 40 m × 40 m, is too coarse for any but general inventory studies at much the same level as that achievable from

---

Description of plate 12

FIGURE 16. Topography, land use and coastal features on SIR-A imagery at nominal 1:1000000 scale; radar illumination is from southward, i.e. from top of each image.

(*a*) Karakoram Range, northwest Pakistan/southwest China (data-take 32/33). Peaks of typically 8000 m in the highest part of the Himalayas. Although lay-over and foreslope brightening are widespread and occasionally severe, there is little interfering radar shadow. The high altitude of the sensor results in an even illumination across the swath even in mountainous terrain; morphological detail, e.g. glaciers, is good although the content of bedrock geological data is poor. The thick snow of the whole area is apparently completely penetrated by the L-band radar.

(*b*) Kuh-e-Sahand/Boz Dagh (3700 m) volcano, Tabriz, northwest Iran (data-take 35/36). A massive Quaternary andesite volcano (over 5000 km^2) with several cones, mostly of dacite. Tuffs and ashes occupy the lower slopes. The Kuh-e-Choruglu Neogene basalt volcano (on right) is surrounded by the lake of Daryacheh Yerezaiyeh (top right corner).

(*c*) Mexicali, northern Mexico (data-take 24C). Dense cultivation in semi-arid, low relief area showing fields, roads and towns, and marked difference of field patterns across the U.S. frontier to the north.

(*d*) Brasilia, eastern Brazil (data-take 24C). Roads, buildings, reservoirs, minor drainage channels, forest and cultivated areas show clearly in this example from tropical savannah.

(*e*) Arabian Gulf and Abu Dhabi (data-take 37A). Features offshore Abu Dhabi (large bright aggregate reflexions) include petroleum drilling rigs (bright stellate reflectors) and sea surface disturbance probably influenced by bottom topography.

(*f*) Examples of two dense drainage networks from Rio Meticá, Colombia (data-take 24C), and Shansi Graben, China, upper Huang-ho River (data-take 28).

TABLE 4. PROPOSED SPACEBORNE IMAGING RADAR PROGRAMMES BEGINNING BEFORE 1990

	N.A.S.A. SIR-B	N.A.S.A. SAMEX	E.S.A. ERS-1	C.C.R.S. Radarsat	Japan S.A. ERS-1	E.S.A./ D.F.V.L.R. SAR facility	Dornier M.R.S.E.
expected launch	1984	1987	1988	1990	?1990	?1986	?1983–1984
orbit altitude/km	225	225	675	1000	570	250	—
orbit inclination	57°	57° and polar	quasi-polar, Sun-synchronous; high angle; 3 day cycle	inclined polar, Sun-synchronous, 99.5°	?polar, Sun-synchronous	—	—
frequency/ GHz	1.3	?1.3 and 9.6	5.3	—	1.2–1.3	5.3 and 9.6	9.62
wavelength	23 cm (L-band)	L and C synthesized X-band	X (and L?)	5.7 cm (C-band) and possible 23 cm (L-band)	23 cm (L-band)	X, C or simultaneous X-C	C-band
transmitted bandwidth/ MHz	12 (×2)	—	—	—	13	14	—
polarization	HH	HH, HV, VV	HH	—	—	?VV; poss. dual polarization	HH/VV
depression angle	variable	variable	—	—	33°	46° (survey mode); 24° ('pointing' mode)	—
incidence angle (from vertical)	variable, between 15° and 60°, controlled from ground	15–60°	*ca.* 35°	30–45°	—	—	—
image swath width/km	30–60	30–60	75–80	150–250	75	75 or 30+30 for simultaneous X and C	8.5
antenna	folding 8 panels; 4 m stowed; 10.5 m × 10 cm; tiltable	?as SIR-B	*ca.* 10 m × 1 m	16.5 m × 1.5 m	—	folding; 10 m × 1.6 m extended	2 m long
image resolution/m	17–55	?17–55	100 (1 dB) or 30 (2.5 dB)	25–30	25	22–35	25
number of looks	4	—	—	3–4	4	5	—
peak power transmitted/W	1000	—	(mean < 400)	—	1500	—	—
data acquisition time	25 h digital plus simultaneous 8 h optical	—	—	continuous	—	—	—
area covered	31×10^6 km^2 in total	eventually global in several missions	ground track spacing of 900 km at equator; coverage could be increased by changing 3 day repeat cycle ×2 if use both ascending and descending passes; global coverage possible	—	—	—	small

	N.A.S.A. SIR-B	N.A.S.A. SAMEX	E.S.A. ERS-1	C.C.R.S. Radarsat	Japan S.A. ERS-1	E.S.A./ D.F.V.L.R. SAR facility	Dornier M.R.S.E.
recording	digital and optical; digital relayed by TDRSS at 46 Mbit s^{-1}	digital and optical; possible real-time option	digital, at *ca.* 100 Mbit s^{-1}, and optical	direct transmission to 2 receiving stations with SAR processors, in Canada to serve as Arctic Pilot Ice mapping station; onboard recorders have limited space; use of data will need receiving station	optical and digital	digital; data stored on board at 120 Mbit s^{-1} and relayed at 32 Mbit s^{-1}	digital and optical
processing	possible real-time processor by 1985 (all data in 7 days at 15 m resolution); quick-look at 100 m available immediately; full resolution optical processed data need $2\frac{1}{2}$ years to process	—	—	near real-time processing to produce images 4 h after overflight (MDA developing technology)	—	—	—
other equipment	large-format vertical camera with 15 m resolution	—	SAR wave mode; C-band scatterometer, radar altimeter; ocean colour mapper (OCM)	wind–wave scatterometer; optical imaging system/ thematic mapper; scanning microwave radiometer; altimeter	—	—	—
platform	Shuttle	Shuttle; about 4 flights every 6–9 months, missions of 5–7 days each; Spacelab at later date	satellite	satellite with 3–5 year life; 3–4 needed for operations 1990–2000	satellite	Shuttle	Spacelab; now developed into SAR Facility programme; may be incorporated on Shuttle
reference	Carver (1982)	Carver (1982)†	Honvault (1981)	Raney (1982)	Matsumoto *et al.* (1982)	Braun (1982)	Theile (1982)

† N.B. FIREX (free-flying imaging radar experiment) is proposed to follow SAMEX on satellite or Spacelab.

Seasat. Nevertheless there are striking examples of how a radar of SIR-A type could monitor or assist studies in urbanization, forestry and forest-destruction, agricultural development, terrain and geomorphological analysis, development planning, irrigation and others.

Figure 7, showing of the North China Plain near Peking, illustrates the detail achievable by SIR-A as well as giving insight into the dense population of China. The image is a part of two swaths of similar density of towns and villages, over 75 000 km^2. Figure 16*c*, *d*, depicting crop-

lands, contrasts strongly with the remote terrains of figure 16*a*, *b*, *f*. Figure 16*e*, of Abu Dhabi, depicts interesting urban and coastal features.

7. Future spaceborne imaging programmes

The significance of the results from SIR-A is that they illustrate the Shuttle's aptitude for experiment, and probably also for operations, with imaging radars. This was important because there are many questions yet to be resolved as to the optimum spaceborne radar system(s) for monitoring the Earth's land surfaces. The Shuttle appears to be the ideal vehicle with which the necessary experiment can be made. It combines global performance with the opportunity for varying the instrumental parameters.

SIR-B, again with L-band radar, but with variable-depression antenna and digital data transmission, is planned by N.A.S.A. for launch in 1984. This will permit the evaluation of the effect of depression angle in geological, natural vegetation and land-use objectives. The current proposal in N.A.S.A. is that SIR-B should be followed in the second half of the 1980s by a multi-polarization, multifrequency radar. This experiment, SAMEX (Shuttle Active Microwave Experiment) promises to be as important for agricultural and land-use purposes as for geological studies. It may not be until SAMEX flies that an overland operational radar satellite can be justified.

The E.S.A., the Canadian Centre of Remote Sensing (C.C.R.S.) and the Japanese Space Agency have major satellite imaging radar programmes planned during the 1980s. Summary details are given in table 4.

Multifrequency and multipolarization radar imaging will feature more prominently in future spaceborne programmes. The necessity of this for agricultural purposes has been demonstrated in the E.S.A.'s recent SAR-580 SLAR campaign (E.S.A./J.R.C. 1982; Haskell & Sorensen 1982), which was undertaken as part of the planning for the E.S.A.'s ERS-1 satellite. A U.K. example of the SAR-580 campaign (figure 2*a*) clearly demonstrates the usefulness of *both* X and L bands over land.

Another example reported by Sieber & Trevett (1982) demonstrates the potential that multifrequency and multipolarization imaging radars will have in crop discrimination. They produced co-registered images from the Oberpfaffenhofen test site of DFVLR. These considerably improved crop discrimination, the most effective image being the composite of the three frequencies X, C and L bands in VV polarization.

8. Discussion

The usable information content of commercial SLAR, Seasat and SIR-A (table 5) is large over land, especially at regional scales. The all-weather day and night capability of imaging radar, coupled with its sensitivity to surface slope, roughness and moisture, makes it an ideal complement to Landsat.

From approximately 18×10^6 km^2 of commercial SLAR imaging and many test-site investigations there has not seemed to be a firm consensus on the parameters most suitable for spaceborne radar. One of the problems in reaching consensus is that there are competing requirements between land and sea operations and between geology and land-use applications. Seasat and SIR-A confirmed the usefulness of L-band to applications *over land*. SIR-A showed that a moderate

radar inspection angle (about 47° from vertical) produced image characteristics useful over a diversity of terrain, environment, vegetation and geology. Other wavebands, polarizations, depression angles, etc., remain to be tested in space.

SIR-A studies focus attention on five interpretational requirements for spaceborne radars *over land.*

1. *Repeat coverage.* Repetition of coverage is desirable for monitoring crops, for example, but for geological purposes a once-only cover or a repetition for different seasons, to permit multi-temporal comparisons, is all that is necessary. A long-cycle repetition, perhaps every 6–12 months, could also be useful to monitor desertification and hydrogeological changes and deforestation. SIR-A demonstrated that L-band could be particularly useful in desertification studies.

TABLE 5. SUMMARY COMPARISON OF PRINCIPAL CHARACTERISTICS OF SEASAT AND SIR L-BAND (23 cm) IMAGING RADARS

	Seasat	SIR-A	SIR-B
orbit inclination/deg	polar, 108	Shuttle, 38	Shuttle, 57
altitude/km	794	268	225
radar frequency/GHz	1.275	1.272	1.282
radar pulse bandwidth/MHz	19	6	12
swath width/km	100	55	variable, 30–60
incidence angle/deg	20	47	variable, 15–60
range resolution/m	25	40	variable, 55–17
number of looks	4	7	4
processing	optical and digital	optical only	optical and digital
attributable cost/$M	400	9	?13 (exclusive of launch costs)

Global coverage could be achieved relatively quickly. Thome (1982), for example, calculates that the total *overland* Earth, about 145×10^6 km^2, could be sensed from polar orbit in 24 days, to provide image swaths 100 km wide with a 30 km side overlap (for 'stereo'; see Kaupp *et al.* (1982*b*)).

2. *Resolution.* For geological purposes the image interpretation matches the resolution available. The 40 m spatial resolution of SIR-A produced images whose appearance were not markedly different from those of Seasat, even though the latter had 25 m resolution. For land-use purposes higher spatial resolution is needed for discrimination; although not as important for geology, geological interpretation would benefit from improved resolution.

3. *Image swath.* A swath of 50–100 km seems best to accommodate requirements for reasonably rapid regional coverage. The ideal imaging mode is probably a combination of simultaneous wide-swath moderate-resolution image with a narrow-swath (say 5–10 km) high-resolution (10 m or better) image.

4. *Radar frequency.* A combination of frequencies is probably the most important interpretational requirement. X and L bands have been widely tested, and experiments have also shown C-band to have merit. L-band with its lower power requirement proved itself on Seasat and SIR-A. However, single-band images constrain interpretation, particularly in land-use applications. Multifrequency and multipolarization radar would permit better discrimination of lithological, vegetational and surface types. Experiments from space are needed to confirm the benefits to interpretation.

5. *Geometry.* Qualitative interpretation of radar images is dominated by recognition of

texture, shape and context. For geology there seems to be a side latitude of direction and inspection angle of radar illumination that is tolerable. Distortion rules out useful imagery over high-relief terrain, although the even illumination and consistent moderate inspection angles from space by SIR-A produced more acceptable images over high relief than those produced by SLAR. Varied inspection angles, especially over low relief and over large diverse areas rather than individual targets, need to be tested in conjunction with different frequencies.

N.A.S.A.'s SIR programme, and others, have been addressing the task of defining these requirements; the Shuttle offers an excellent vehicle to study them further. It maintains flexibility of payload, coverage and system parameters, allowing incorporation of technological development and providing extensive regional coverage over diverse terrain at relatively moderate cost. SIR-B and SAMEX will enable the testing and selection of the most appropriate system parameters (for both land and sea operations) before commitment to dedicated fully operational satellites.

The directors of Hunting Geology and Geophysics Limited authorized the publication of this paper. Hunting are joint official observers with the Royal Aircraft Establishment, Farnborough, to the SIR-A investigation team. SIR-A imagery reproduced here has been prepared by Hunting from optically correlated positive film transparencies supplied by the Jet Propulsion Laboratory, Pasadena.

REFERENCES AND SELECTED BIBLIOGRAPHY

Anon. (Various dates, 1970s and 1980s) *Projecto RADAM* (Multivolume reports covering geology, geomorphology, soils, vegetation and landuse). Rio de Janeiro: Ministerio das Minas e Energia. Summary maps at 1:1 000 000 scale, regional maps (in part) at 1:500 000 and 1:250 000 scales.

Arnold, H. J. P. 1981 *Br. J. Photogr.*, 9 Oct., pp. 1031–1041.

Azevedo, L. H. A. 1971 In *Proc. 7th Symp. Remote Sensing of Environment, ERIM, Univ. of Michigan, Ann Arbor*, vol. 3, pp. 2303–2306.

Black, R. *et al.* 1979 *Geol. Rdsch.* **68**, 543–564.

Blom, R. *et al.* 1982 In Keydel (1982), FA-6, pp. 9.1–9.6.

Blom, R. G. & Daily, M. 1982 *IEEE Trans. Geosci. Remote Sensing*, **GE–20**, 343–351.

Braun, H. M. 1982 In Keydel (1982), WP-9, pp. 1.1–1.6.

Bryan, M. L. 1973 *Radar remote sensing for geosciences: an annotated and tutorial bibliography*. ERIM, Rep. no. 193500 1-B. University of Michigan, Ann Arbor. (For Nat. Sci. Foundation, Contract no. G1-34089 X.)

Bryan, M. L. 1979 *Bibliography of geologic studies using imaging radar*. J.P.L. Pub. no. 79–53. N.A.S.A./J.P.L.

Carver, K. & Bush, T. F. 1979 *Airborne remote sensing of saline seeps: the 1978 Harding Co., S. Dakota experiment.* (Final Rep. N.A.S.A. Contract no. NAS 9-15421.) New Mexico, State Univ.

Carver, K. R. 1982 In Keydel (1982), TP-7, pp. 1.1–1.6.

Correa, A. C. 1980 In Harrison (1980), pp. 385–416.

Covault, C. 1982 *Aviation Week Space Technol.*, 2 August, pp. 17–18.

Curlander, J. C. 1982 *IEEE Trans. Geosci. Remote Sensing*, **GE–20**, 359–364.

Daily, M. *et al.* 1978 *Geophys. Res. Lett.* **5**, 889–892.

Dellwig, L. F. 1980 In Harrison (1980), pp. 351–364.

Diazgranados, D. A. 1979 *La Amazonia Colombiana y sus recursos. Proyecto Radar grametrico de las Amazonas (PRORADAM)*. (Five volume report including memoir, and maps at 1:500 000 scale, for geology, soils, forestry/vegetation and landuse.) Bogota: Republica de Columbia.

Eberhart, J. 1982 *Science News* **121**, 419–420.

Elachi, C. 1980 *Science, Wash.* **209**, 1073–1082.

Elachi, C. 1982 In Keydel (1982), FA-6, pp. 5.1–5.6.

Elachi, C. *et al.* 1982*a* In Keydel (1982), FA-6, pp. 8.1–8.4.

Elachi, C. *et al.* 1982*b* *Science, Wash.* (In the press.)

E.S.A. 1981 *Synthetic aperture radar image quality: selected papers.* (Workshop ESRIN, Frascati, Dec. 1980.)

E.S.A./J.R.C. 1982 *SAR-580 Campaign 1981.* (Various reports by various authors for European Space Agency/Joint Research Centre.)

Estes, J. E. 1982 In Keydel (1982), FA-6, pp. 7.1–7.5.

Ford, J. P. 1982 In Keydel (1982), FA-6, pp. 6.1–6.6.
Ford, J. P. *et al.* 1980 *Seasat Views North America, the Caribbean, and Western Europe with imaging radar.* J.P.L. Pub. no. 80-67. N.A.S.A./J.P.L.
Froidevaux, C. M. 1980 In Harrison (1980), pp. 457–501.
Guyenne, T. D. & Lévy, G. (eds) 1981 *Coherent and incoherent radar scattering from rough surfaces and vegetated areas (Proceedings Workshop, Alpbach, Austria, March 1981).* E.S.A. Report no. SP-166. EARSeL/E.S.A.
Harrison, P. (chmn) 1980 *Radar geology: an assessment (Report of the radar geology workshop, Snowmass, Colorado, July 1978).* J.P.L. Pub. no. 80-61. N.A.S.A./J.P.L.
Haskell, A. & Sørensen, B. M. 1982 In Keydel (1982), WA-5, pp. 1.1–1.5.
Held, D. N. *et al.* 1982 In Keydel (1982), WP-8, pp. 2.1–2.6.
Honvault, C. 1981 In *Digest, 1981 International Geoscience and Remote Sensing Symposium (IGARSS '81), Washington June 1981,* pp. 1320–1326. Piscataway, N.J.: Institute of Electrical and Electronics Engineers Geoscience and Remote Sensing Society.
Hubbard, G. 1982 *Oilman,* October, pp. 19–25.
Hunting Geology and Geophysics Ltd. 1981 The evaluation of the data content of overland Seasat SAR imagery. Unpublished report prepared for Royal Aircraft Establishment, Farnborough. Final report. (Two volumes.)
Hunting Technical Services Ltd. 1977 NIRAD Project. Interpretation phase, progress report no. 3 (Digital analysis by Harwell). Federal Department of Forestry, Government of Nigeria.
Hunting Technical Services Ltd. 1978 NIRAD Project. Interpretation phase. Summary. Government of Nigeria.
Kaupp, V. H., Waite, W. P. & MacDonald, H. C. 1982*a* *IEEE Trans. Geosci. Remote Sensing* **GE–20**, 383–390.
Kaupp, V. H. *et al.* 1982*b* In Keydel (1982), TA-4, pp. 2.1–2.5.
Keydel, W. (ed.) 1982 In *Digest, 1982 International Geoscience and Remote Sensing Symposium (IGARSS '82), Munich, June 1982.* (Two volumes.) Piscataway, N.J.: Institute of Electrical and Electronics Engineers Geoscience and Remote Sensing Society.
Kobrick, J. 1982 *Astronomy,* August, pp. 18–22.
Lawrence, G. M. & Martin-Kaye, P. H. A. 1983 (In the press.)
Leberl, F. 1978 *ITC-Delft J.,* pt 1, pp. 167–190.
Leberl, F. W. 1980 In Harrison (1980), pp. 307–335.
de Loor, G. P. 1982 In Keydel (1982), TP-1, pp. 1.1–1.7.
Luther, C. A. *et al.* 1982 In Keydel (1982), TA-8, pp. 1.1–1.9.
McCandless, S. W. & Miller, B. P. 1975 *Acta astronaut.* **2**, 771–783.
MacDonald, H. C. 1980 In Harrison (1980), pp. 23–37.
MacDonald, H. C. & Waite, W. P. 1971 *Mod. Geol.* **2**, 179–193.
MacDonald, H. C. & Waite, W. P. 1973 *Mod. Geol.* **4**, 145–158.
McDonough, M. M. & Deane, G. D. 1979 In *Workshop Seasat SAR processor* (E.S.A. Rep. no. SP-154), pp. 9–18.
McDonough, M. M. & Martin-Kaye, P. H. A. 1983 *Int. J. Remote Sensing.* (In the press.)
McDonough, M. M., Martin-Kaye, P. H. A. & Deane, G. D. 1983 In *Proc. Symp. 'Seasat over Europe', Royal Society, April 1982.* EARSeL. (In the press.)
Martin-Kaye, P. H. A. 1973 In *Environmental remote sensing: applications and achievements. (Symp. Bristol, October 1972)* (ed. E. C. Barrett & L. F. Curtis), pp. 30–48. Edward Arnold.
Martin-Kaye, P. H. A. 1980 In Ackermann, F. (Ed.), *4th International Soc. Photogramm. Congress, Hamburg, July 1980 (Int. Arch. Photogramm.* **23** (B8), Comm. 7) (ed. F. Ackermann), pp. 624–633.
Martin-Kaye, P. H. A. & Williams, A. K. 1973 In *Memoria IX Conferencia Inter-Guyanas, Caracas (Bol. Geol., Pub. especial* **6**), pp. 600–605.
Martin-Kaye, P. H. A. *et al.* 1980 In Harrison (1980), pp. 502–507.
Matsumoto, K. *et al.* 1982 In Keydel (1982), TP-7, pp. 2.1–2.5.
Matthews, R. E. 1975 *Active microwave workshop report.* N.A.S.A. Report no. SP-376, Washington, D.C.
Matthews, R. E. 1978 *Active microwave user workshop report.* N.A.S.A. Conference Pub. no. 2030. N.A.S.A./J.S.C.
Moore, R. K. *et al.* 1974 *Application of imaging radars: a bibliography.* Rep. Remote Sensing Lab. no. 265-2, University of Kansas, Lawrence.
Moreira, H. F. 1973 *Controle de qualidade de imagens de radar, Brazil.* (Dept. Nacional Producao Mineral, Projeto RADAM, tech. Rep. no. 57). Rio de Janeiro.
Nagler, R. G. & McCandless, S. W. Jr 1975 *Operational oceanographic satellites: potential for oceanography, climatology, coastal processes and ice.* Pasadena: J.P.L.
National Academy of Sciences 1977 *Microwave remote sensing from space for earth resources surveys.* N.A.S.A. publication no. CR-157891. Washington, D.C.: National Research Council.
Noel, J. & Pelleau, R. (eds) 1973 *Projet SARSAT. Synthese de l'étude des missions.* (Contributions from Sodeteg, Hunting Geology and Geophysics Ltd., B.R.G.M.)
Pala, D., Mussakowski, R. & Wedler, E. 1980 In *14th International Soc. Photogramm. Congress, Hamburg, July 1980 (Int. Arch. Photogramm.* **23** (8), Comm. 7) (ed. F. Ackermann), pp. 754–771.
Paris, J. F. 1982 In Keydel (1982), FA-4, pp. 1.1–1.6.
Parry, D. & Trevett, J. W. 1979 *Geogrl J.* **145**, 265–281.
Raney, R. K. 1982 *The Canadian RADARSAT programme.* In Keydel (1982), TP-6, pp. 3.1–3.6.

Rouse, J. W. Jr (ed.) 1977 *Microwave remote sensing symposium, N.A.S.A./J.S.C., Houston, Texas, Dec. 1977* (and Workshop Rept).
Rouse, J. W. Jr 1982 In Keydel (1982), TP-1, pp. 3.1–3.5.
Sabins, F. F. Jr *et al.* 1982 *Bull. Am. Ass. Petrol. Geol.* **64**, 619–628.
Schaber, G. G. *et al.* 1976 *Bull. geol. Soc. Am.* **87**, 29–41.
Schlude, F. 1981 In Guyenne & Lévy (1981), pp. 29–30.
Sieber, A. J. 1982 In Keydel (1982), TA-1, pp. 5.1–5.3.
Sieber, A. & Trevett, J. W. 1982 *IEEE Geosci. Remote Sensing J.* (in the press.)
Taranik, J. V. 1982 In Keydel (1982), FA-6, pp. 1.1–1.5.
Taranik, J. V. & Settle, M. 1981 *Science, Wash.* **214**, 619–626.
Theile, B. 1982 In Keydel (1982), WA-7, pp. 1.1–1.6.
Thome, P. G. 1982 In Keydel (1982), WA-9, pp. 3.1–3.5.
le Toan, T. 1981 In Guyenne & Lévy (1981), pp. 99–110.
le Toan, T. 1982 In Keydel (1982), TP-1, pp. 3.1–3.5.
Ulaby, F. T., Moore, R. K. & Fung, A. K. 1982 *Microwave remote sensing – active and passive.* (Three volumes.) Remote Sensing Laboratory, University of Kansas.
Walters, R. L. 1968 *Radar bibliography for geoscientists.* C.R.E.S. Report no. 61-30, University of Kansas, Lawrence.
Wing, R. S. 1971 *Mod. Geol.* **2**, 1–21.
Wing, R. S. & Dellwig, L. F. 1970 *Tectonic development of the eastern Panamanian Isthmus as revealed through analysis of radar imagery.* (Annual Meeting, Geological Society of America, November 1970.)
Wing, R. S. & MacDonald, H. C. 1973 *Bull. Am. Ass. Petrol. Geol.* **57**, 825–840.

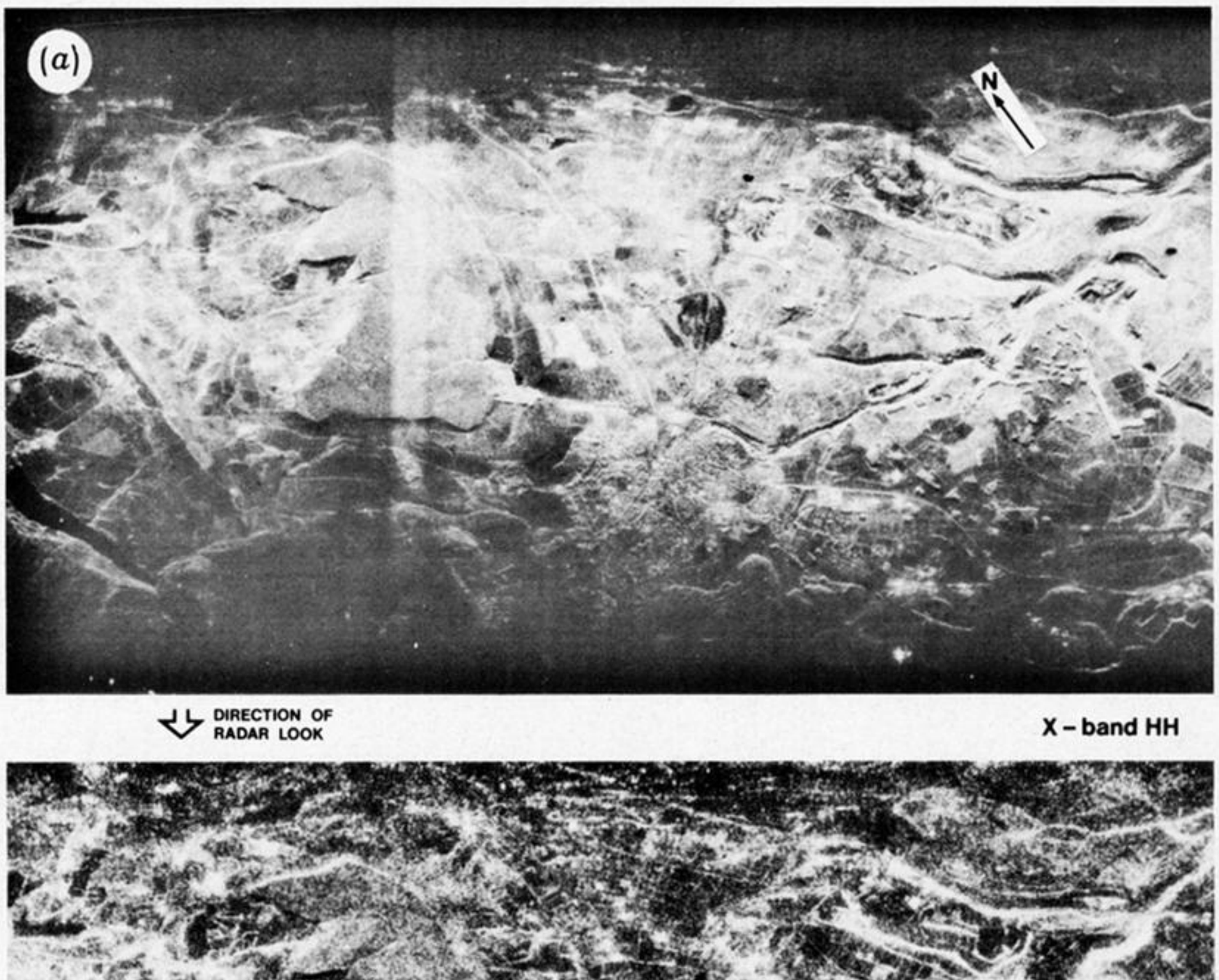

FIGURE 2. (*a*) Comparison of SLAR bands X (3 cm) and L (23 cm), Buxton, U.K., SAR 580. Optical correlated imagery. Scale approximately 1:100000. Resolution is 1.5 m × 2.1 m for X-band and 3 m × 5 m for L-band. The mesa-like hill is formed from mid-Carboniferous gritstone more or less horizontally bedded and covered by a thin blanket of hill peat and moorland low scrub. Buxton, dry-stone walls, roads, trees, quarries are well represented on both X and L images, although X-band better delineates individual radar reflectors. The generalization of features on L-band can help rapid recognition of features, e.g. stands of trees, the outline of Buxton.

(*b*) Seasat image of mountains and glaciers in Greenland. The direction of look is from the top of the image; 'chevrons' and conspicuous layover (see particularly the layover of the mountain peaks adjacent to the glaciers) are produced by the steep depression angle of Seasat.

EUROPEAN SPACE AGENCY-EARTHNET-ROYAL AIRCRAFT ESTABLISHMENT

SEASAT 1-RADAR MOSAIC

UNITED KINGDOM

Synthetic Aperture Radar (S.A.R.)
Acquired by The Royal Aircraft Establishment
Receiving Station: Oakhanger England
From N.A.S.A. SEASAT 1 Satellite
Optical Correlation by Environmental
Research Institute of Michigan U.S.A. (E.R.I.M.)

Mosaic constructed by Hunting Surveys Ltd.
Elstree Way Borehamwood Hertfordshire
WD6 1SB England

Mosaic Sponsored By
The Natural Environment Research Council
Polaris House
North Star Avenue
Swindon SN2 1EU

FIGURE 3. Seasat radar mosaic of the United Kingdom and adjacent Ireland, constructed by Hunting Surveys Limited for the R.A.E./E.S.A.-Earthnet and N.E.R.C. (N.A.S.A.'s Seasat 1 SAR data acquired at R.A.E. Oakhanger and optically correlated by E.R.I.M., U.S.A.).

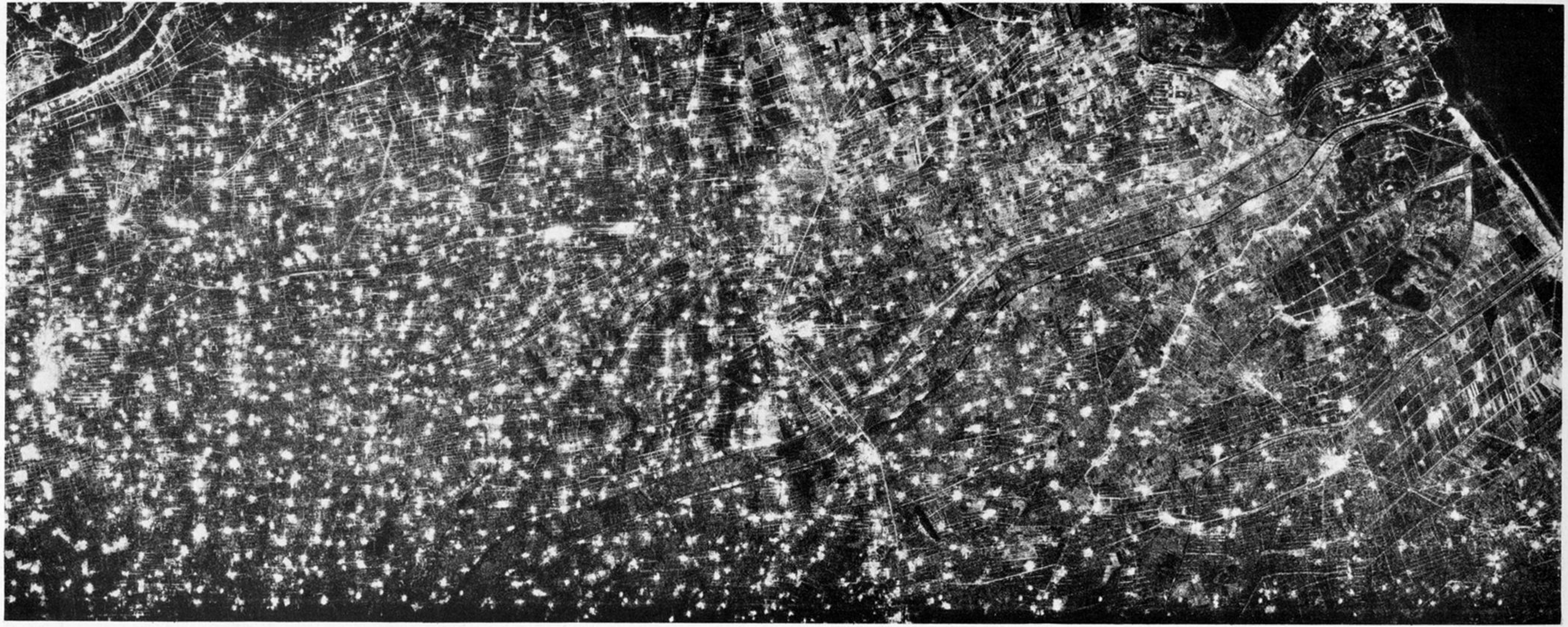

FIGURE 7. SIR-A image (data-take 7) over densely populated and cultivated alluvial/loess plain of north China, near Peking. Nominal scale 1:500000. The bright reflectors are towns and villages. Roads and tracks show clearly from the black tones of flat waterlogged fields. North is to bottom of image.

FIGURE 8. SIR-A swath 29/30 over Adrar des Iforas, northeast Mali. Scale nominally 1:500 000. Bright areas are rough-surfaced outcropping rock; black tonal areas are thick sand. 'Younger Granite' ring-intrusions and associated dyke-swarms and the Iforas granulite unit are particularly distinct. The radar illumination is from top of image, north is to bottom left corner. The area of the subscene in figure 9*b* is shown. The margins are not rectangular because the subscene has been 'warped', on an image processor, to co-register with Landsat.

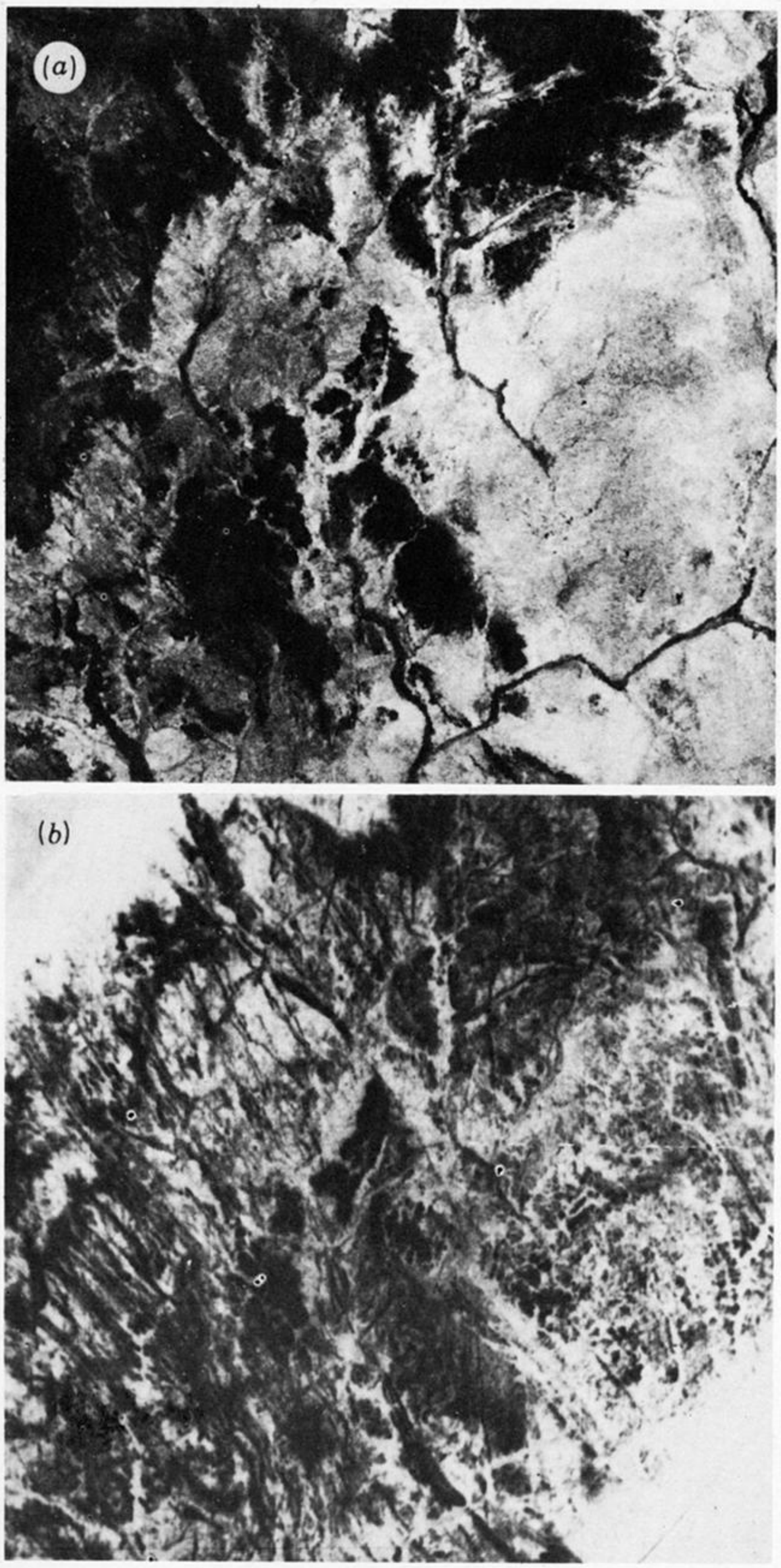

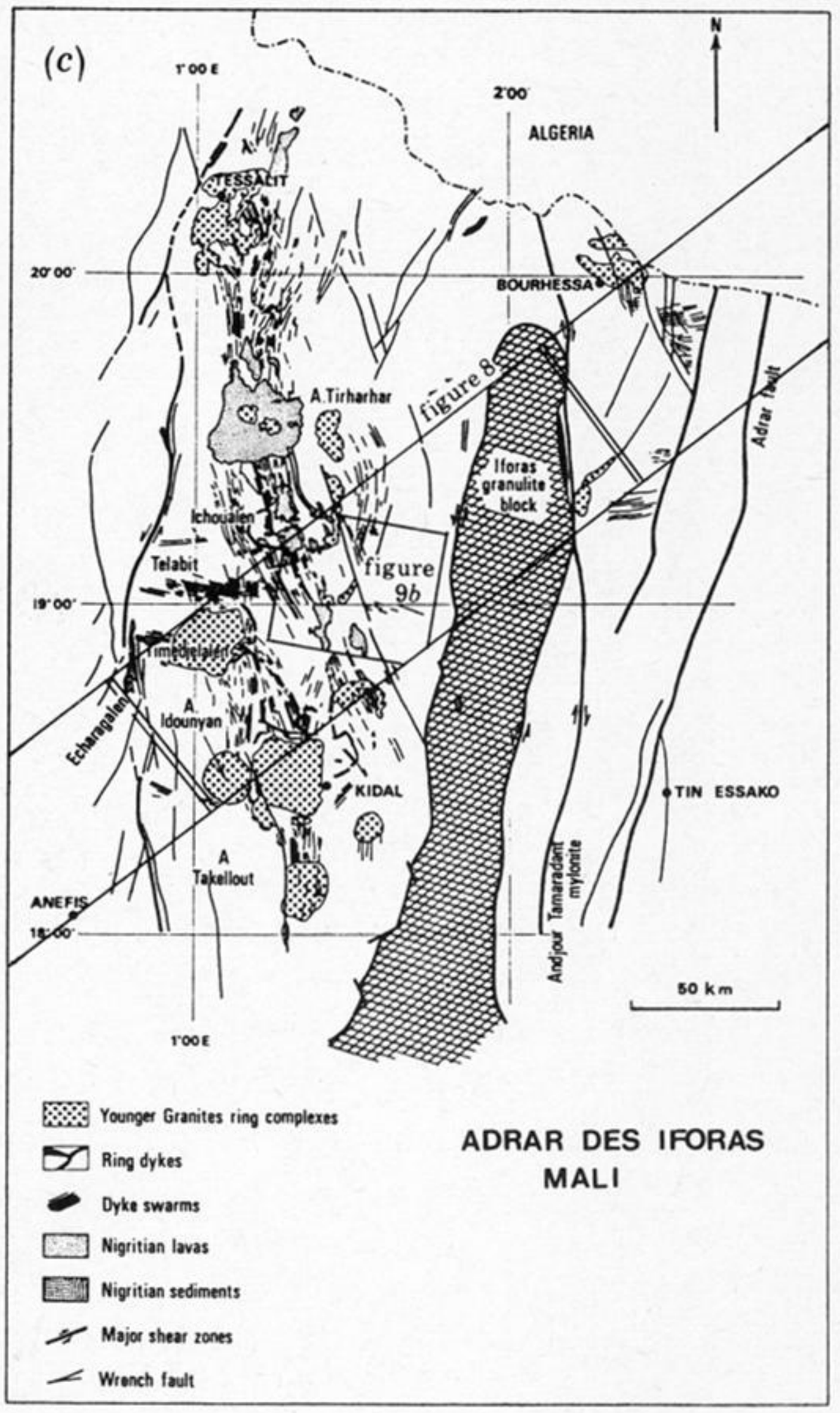

FIGURE 9. (*a*) Adrar des Iforas; Mali Landsat MSS subscene enhanced and warped to co-register with SIR A image on Hunting's image processor (reproduced in monochrome).

(*b*) Equivalent SIR-A image reproduced as negative (bright radar tones reversed to appear black). The bright-reflecting low-relief sand/gravel areas of the Landsat compare with minor drainages and outcrop and perhaps sub-outcrop on the SIR-A (especially the bottom right corner). The dyke swarm shows much more clearly on the SIR-A and a possible small circular feature is identified within a larger circular (top left). The SIR-A imagery responds to small outcrop and boulders better, resulting in more detail, than Landsat because of the former's better resolution (40 m × 40 m compared with 50 m × 80 m for Landsat) and its response to surface roughness. In this very dry area there is also possible shallow penetration and backscatter return of the SIR-A radar beam from subsurface bedrock.

(*c*) Geological sketch of Adrar des Iforas, northeast Mali, showing SIR-A swath (data-take 29/30) and subscenes of figures 8 and 9*b*. (After Black *et al.* (1979).)

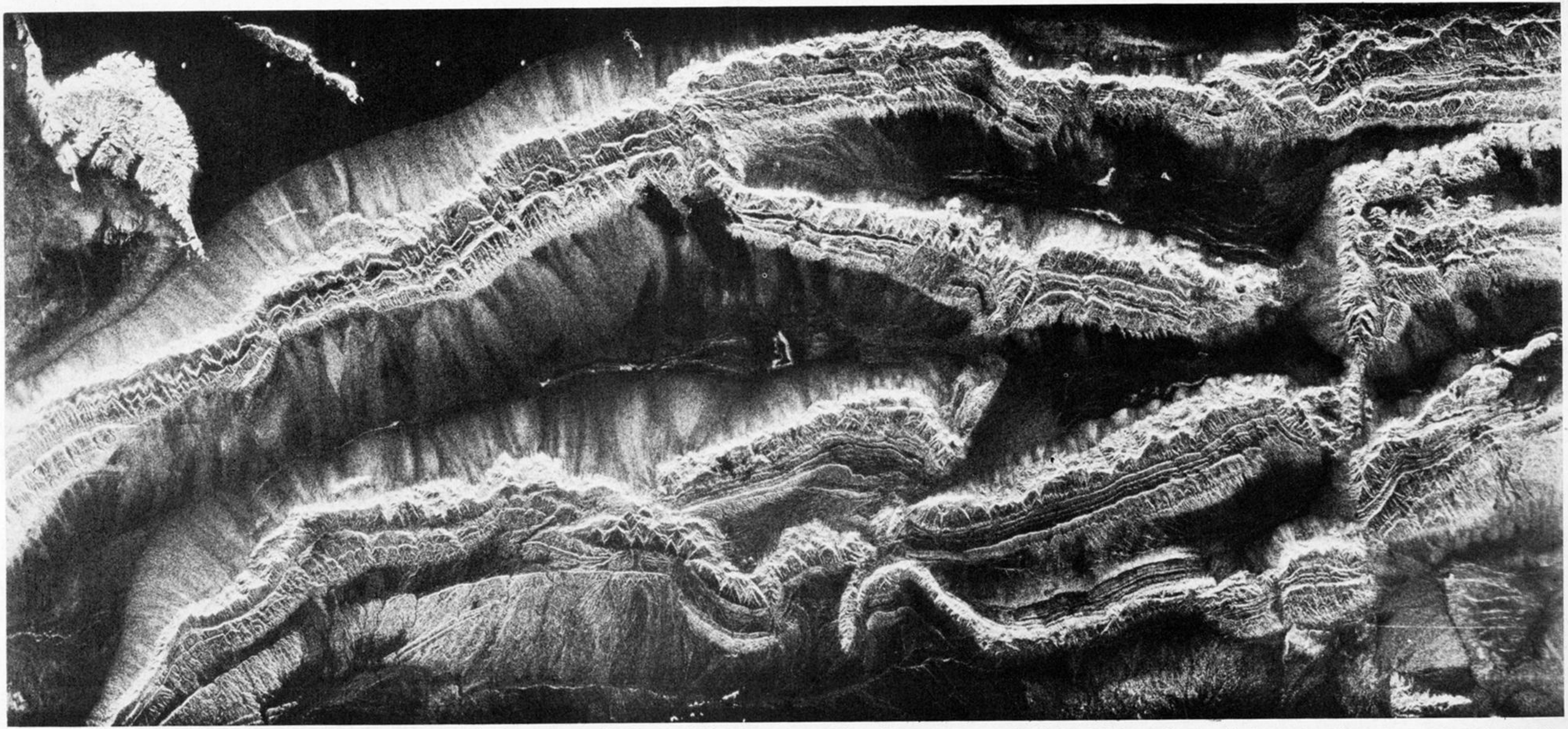

FIGURE 10. SIR-A image (data-take 28) over Kelpin Tagh, western Sinkiang, China, between Tien Shan ranges and Takla Makan desert. Scale approximately 1:500 000. In this arid area folded and thrusted sedimentary rocks are cut by prominent transcurrent faults. Thrust planes dip northward (towards bottom of image). Large cuestas are surrounded by alluvial fans whose rough cobble and boulder surfaces provoke a bright radar response. The boundary between fans and desert sands, which have almost no radar backscatter, is distinct (top left of image). Radar illumination from top of image at approximately 50° incidence angle; north is approximately to bottom left of image. The white dots are fiducial marks representing each second of the Shuttle's orbit.

FIGURE 11. Landsat MSS band 7 image over Kelpin Tagh, western Sinkiang, China. Landsat path/row 159/32, 15 May 1973, centre point N 40° 25′, E 78° 17′. Sun elevation 59° from southeast (top left-hand corner). The better resolution and depiction of surface roughness of the SIR-A results in better definition compared with Landsat.

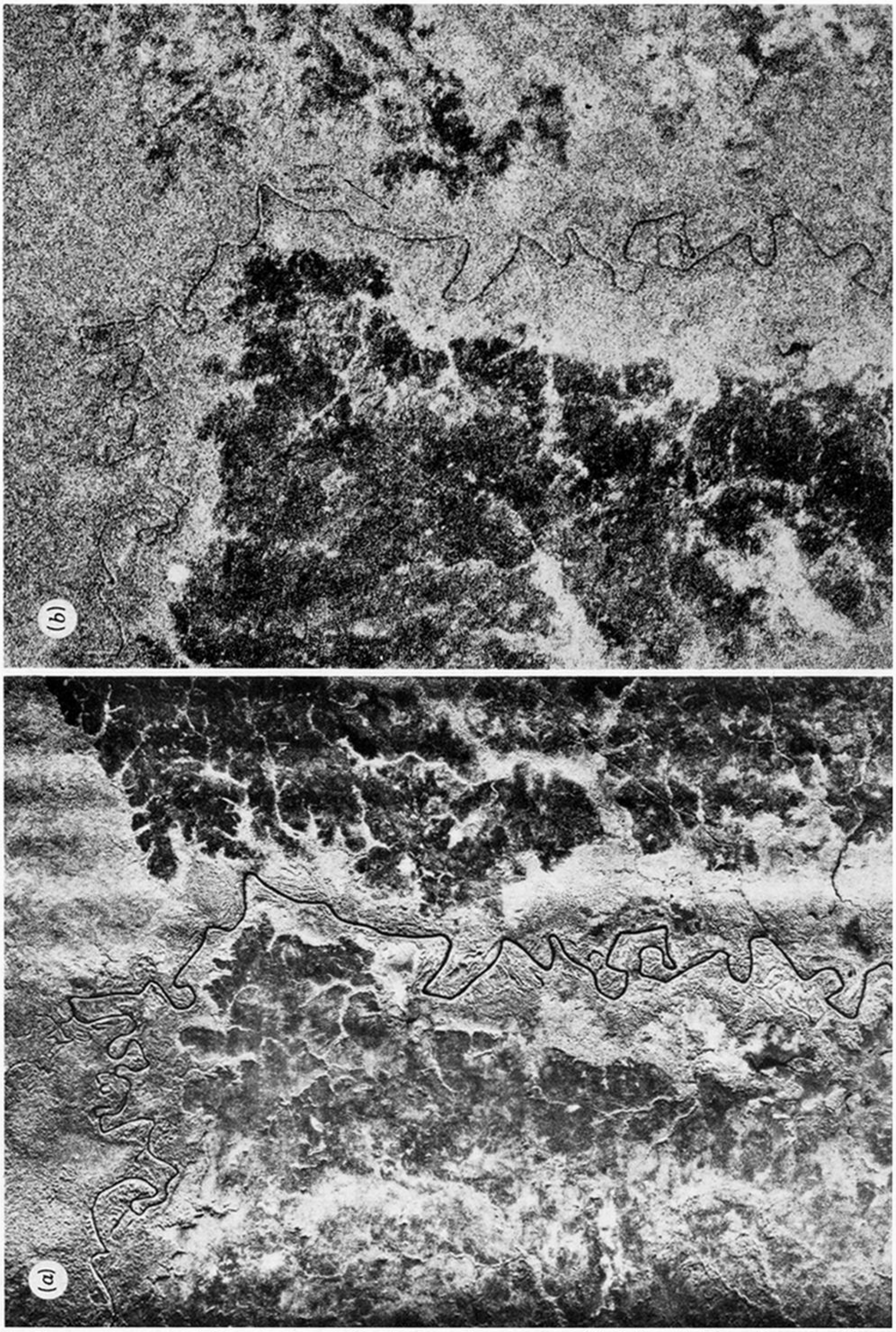

FIGURE 12. Comparison of (*a*) Westinghouse Ka (0.86 cm) SLAR and (*b*) L-band (23 cm), SIR-A (data-take 24C) over low-relief area of northeast Nicaragua. Scale nominally 1:200000. Area of forest and cleared forest savanna underlain by clays and gravels. Although the SIR-A has distinctly inferior resolution (40 m compared with 10 m) laterite-surfaced roads can show well. Differences of tone on the imagery are thought to be due to temporal changes (the two images are 10 years apart, but both of wet season) rather than radar wavelength differences. The dark interfluve areas are probably waterlogged savannah. The radar illumination is from the right-hand side of the image for the SLAR, at an incidence angle of *ca.* 60°; that for the SIR-A is from the top left-hand corner of the image at an incidence angle of 50°. Note that the marked difference of radar illumination and depression angle do not materially change the delineation of radar geological units.

Note added in proof 16 (*March* 1983). Radar depression angle is, of course, substantially variable across the SLAR swath (*a*), being larger in near range (right-hand side) and smaller in far range. The depression angle at centre of swath is equivalent to that of SIR-A but from approximately the opposite direction. The cleared-forest grasslands appear darker at the larger depression angle of the near range of SLAR. The SIR-A (*b*) may be showing a similar but smaller effect in the reverse direction; the depression angle variation across swath of SIR-A is only 5–6° compared with the 30–40° of SLAR.

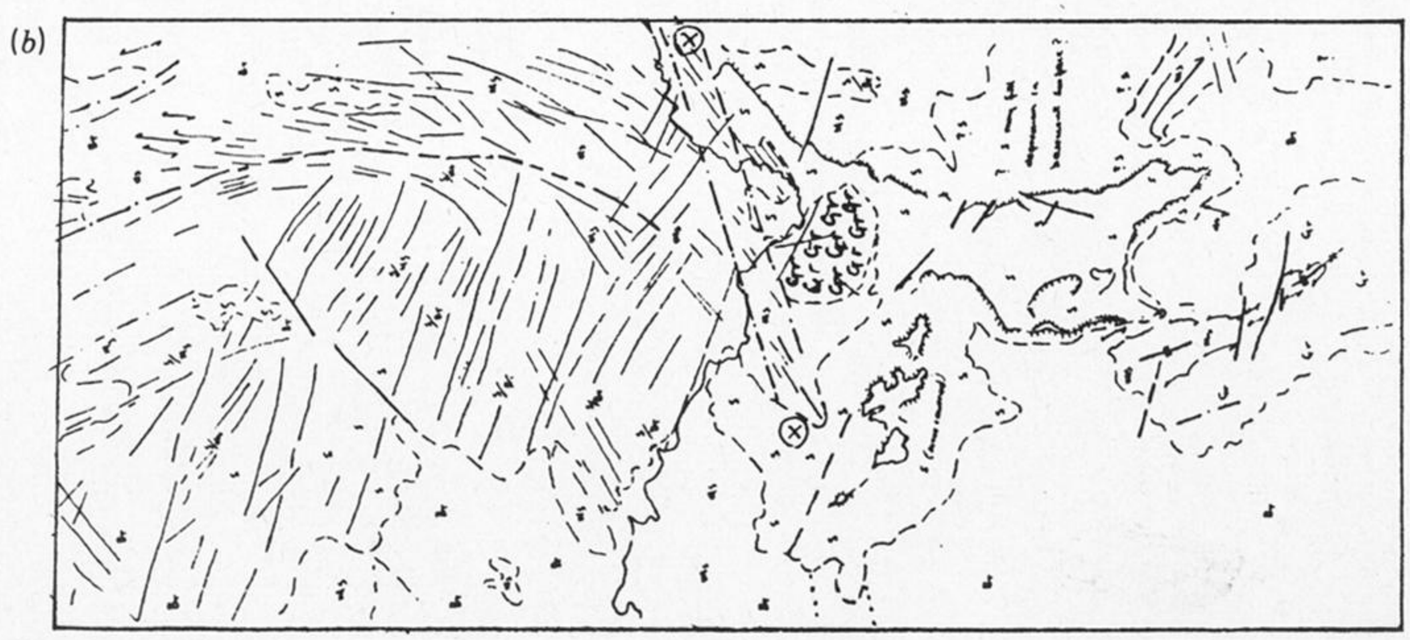

FIGURE 13 (*overleaf*). (*a*) SIR-A image (data-take 34) over part of southern Amazonas, Rio Uaiauka, Venezuela. Nominal scale 1:500000. Inaccessible low-relief area of tropical rain forest underlain by well fractured rocks (left) mapped as acid extrusive rocks set in Lower–Mid-Proterozoic granites and migmatites of the Guiana Shield. The pronounced circular feature is probably a granite ring-intrusion (not shown on maps). The distinct mesa-like form comprises probable Lower Roraima Formation (or an older unit) arenites of ?Mid-Proterozoic age, draped, and possibly gently warped, over the older rocks. Remnants of the tabular arenites on the well fractured Basement rocks account for the preservation of these older rocks. A faulted fold of metasediment or volcanic horizon emerges prominently from featureless Basement rocks (bottom right). Note that the image over this forested area contains no direct radar-signature of lithologies. Context, morphology and inferred geological structure impart, however, substantial indirect information on lithology. The scarp of the Lower Roraima is emphasized by its being perpendicular to the radar signal. The white dots are fiducials representing each second of the Shuttle's flight. Radar illumination is from the top of the image and north is to the bottom left corner.

(*b*) Preliminary geological interpretation of (*a*) at 1:000000 scale. X, Rio Maraca shear zone in Basement. Full key given in the legend to figure 14.

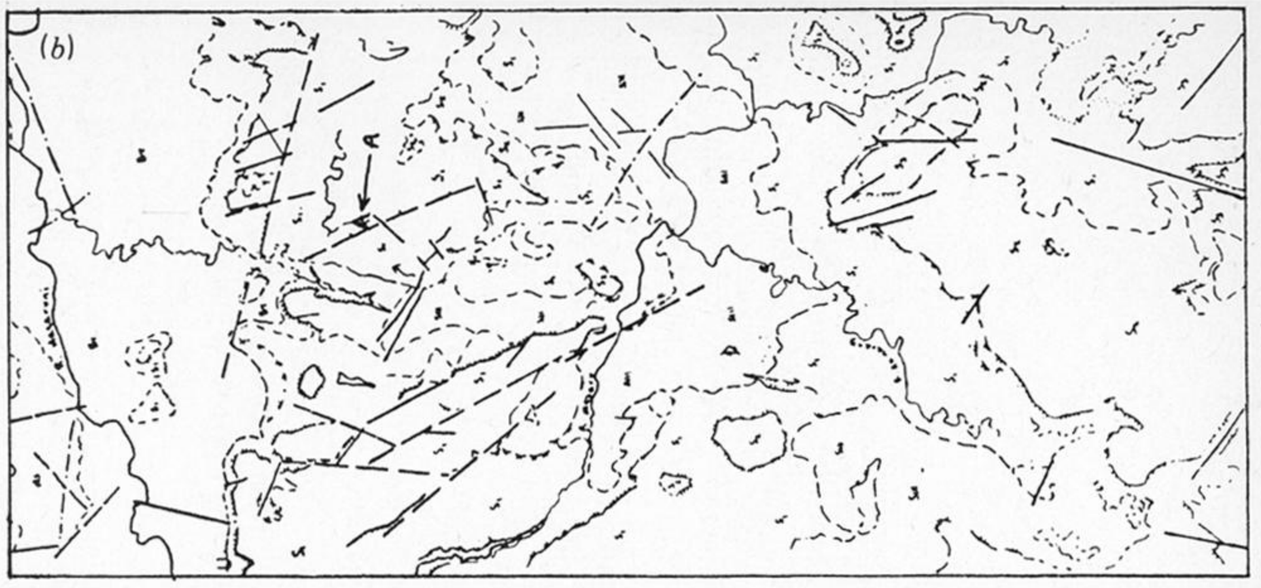

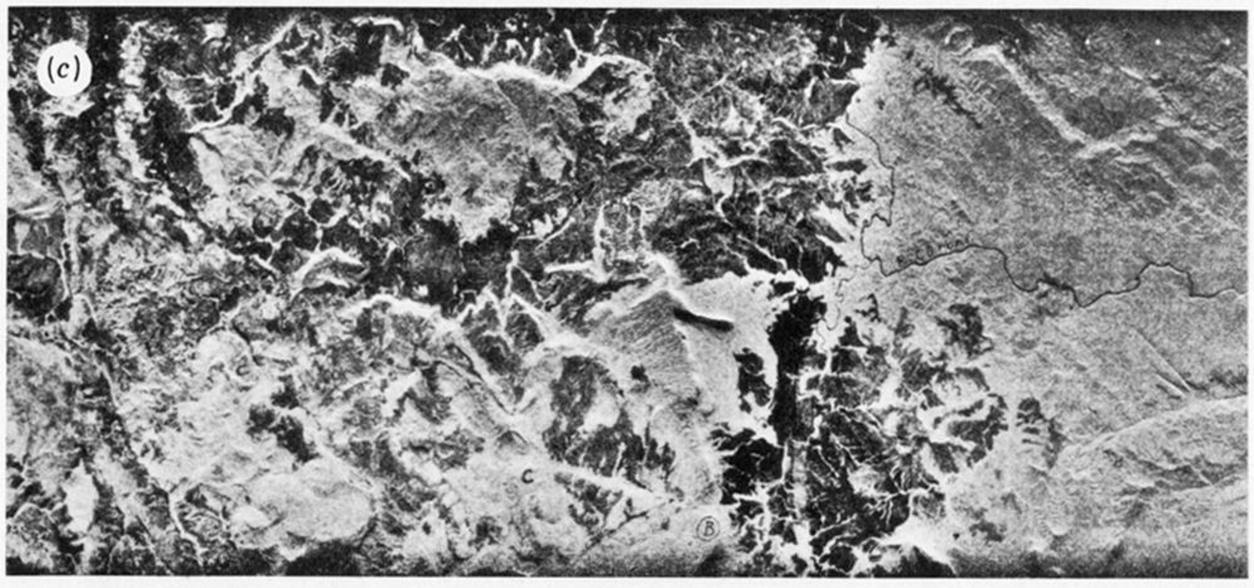

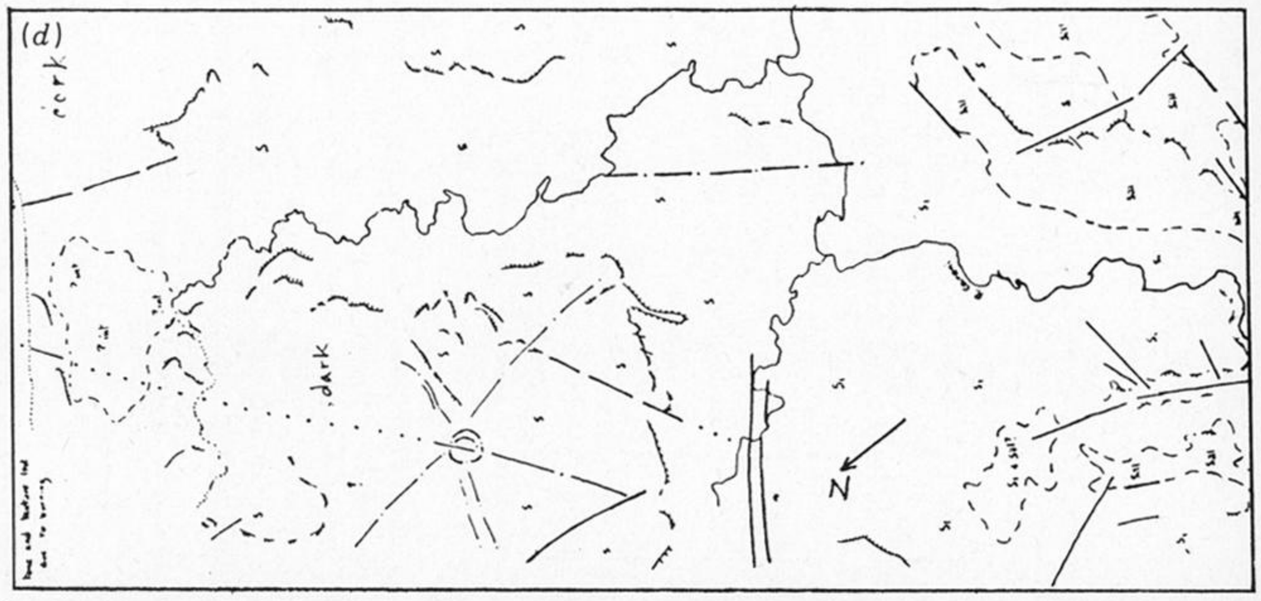

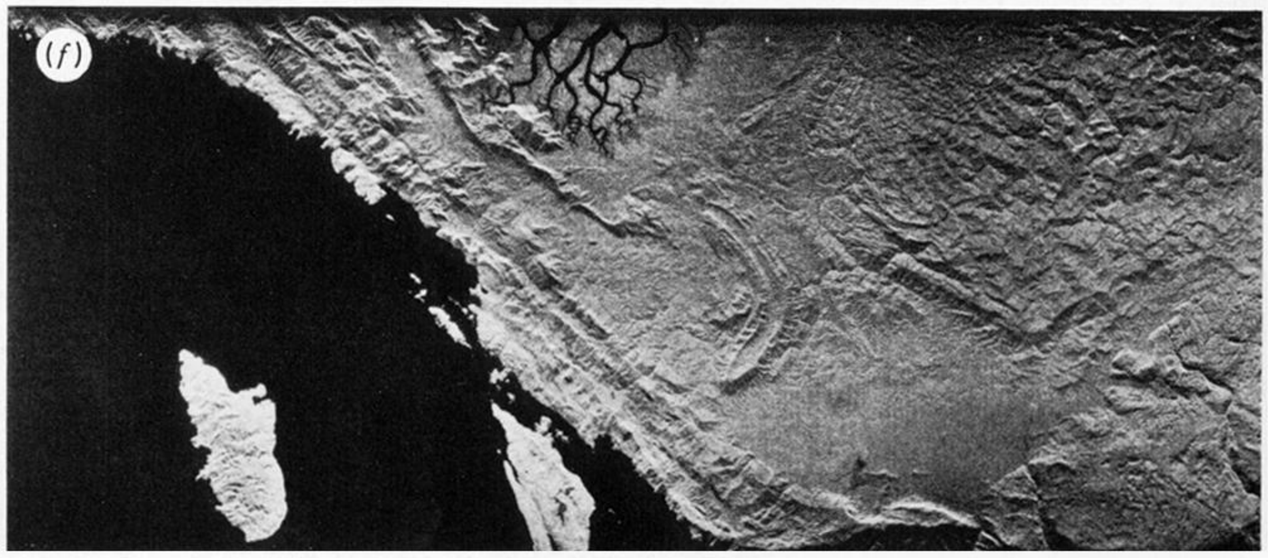

FIGURE 14. SIR-A over tropical regions at nominal 1:1 000 000 scale; radar illumination is from approximately southward, i.e. from top of each image.

(*a*, *b*) Western Guyana and eastern Venezuela (data-take 34). Forested Pakaraima Mountains and River Mazaruni Basin. Proterozoic clastic arenites of Roraima Formation form massif slabs with steep scarps; basaltic sills at A and partly waterlogged savannah (dark low relief areas) of La Gran Sabana at B Low ground on left underlain by gneisses of Guiana Shield.

(*c*, *d*) Eastern Venezuela (southeast Bolivar), and La Gran Sabana and Rio Caroni (data-take 34). Dark areas are partly waterlogged upland plateau savannah at 1000–1500 m. Note strong linear fracture A-B-A′ and circular features at C. Alluvial diamonds in the region have not been traced to source and one can speculate that these circular features are traces of kimberlite intrusion.

(*e*) Mid-Amazon Basin, Brazil (data-take 24C). Dense rain forest and subtle traces of ?Carboniferous sediments.

(*f*) Lengguru fold belt, Vogelkop Peninsula, west Irian (data-take 32/33). Folded Tertiary sediments in dense tropical rain forested mountains.

Key to figures 13*b* and 14*b*, *d*. S, sedimentary formations, subscript indicates superposition, S_1 being oldest. Roraima arenaceous formations. Ms, Precambrian metasediments; d, dykes; sill, basaltic sills of Roraima Formation; int, igneous intrusions; Gr, Precambrian granitic plutons; Gns, Precambrian gneiss; BT, deeply weathered 'Basement' migmatites and granites, etc., masked by lateritized soils and vegetation.

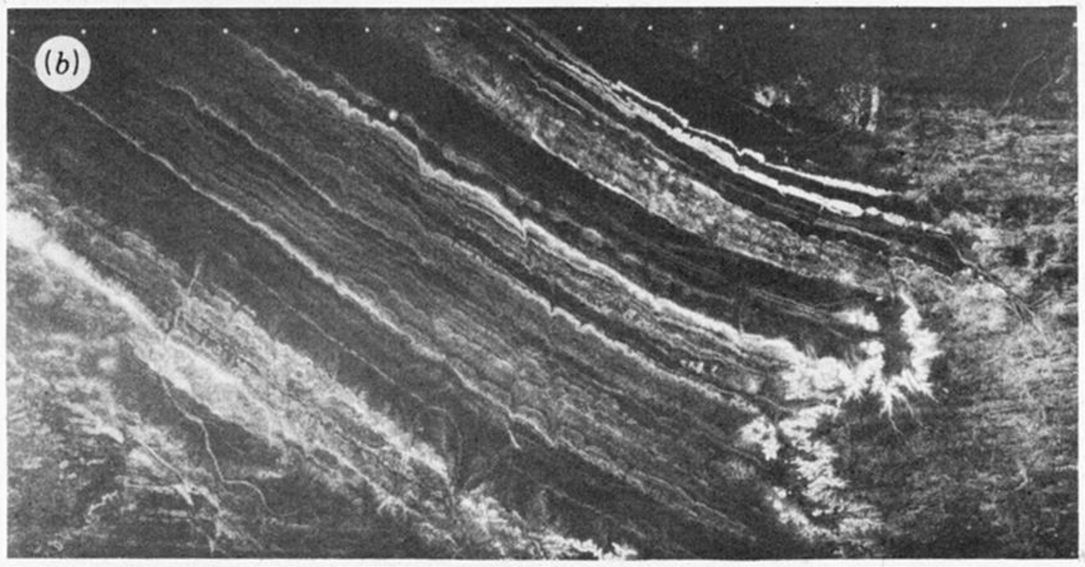

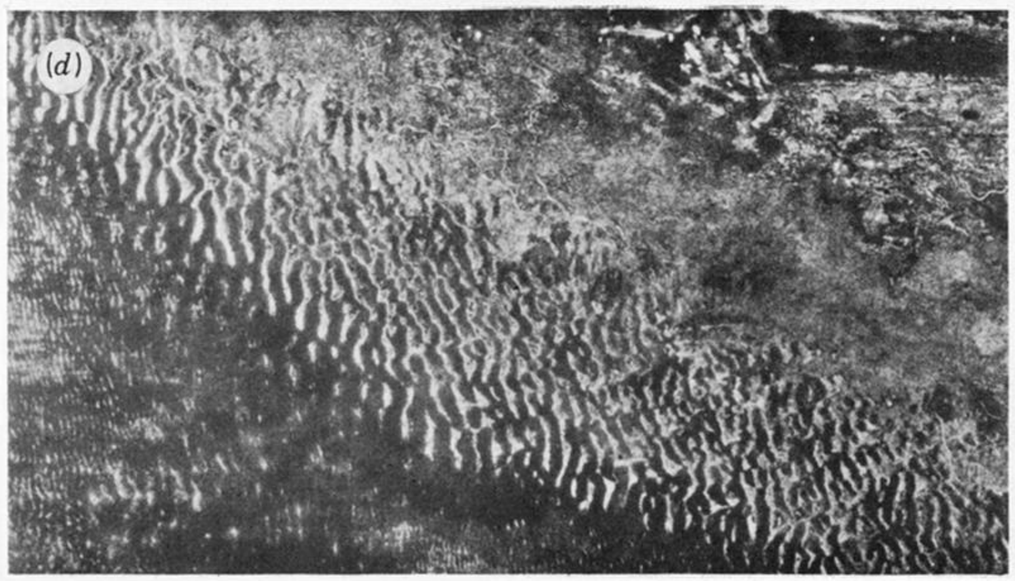

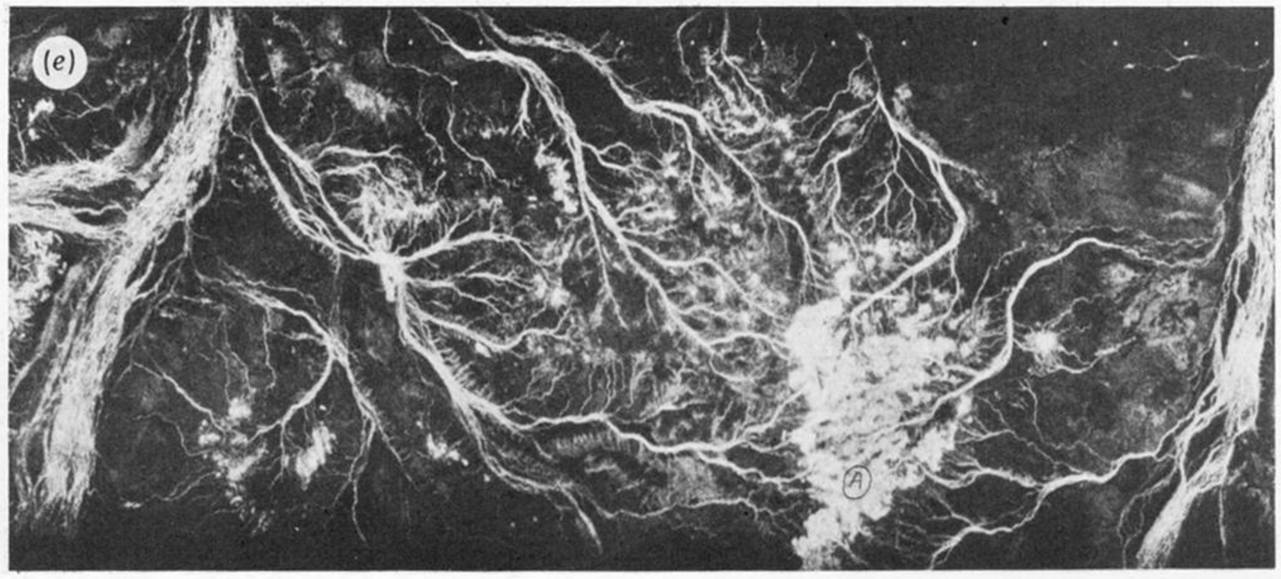

FIGURE 15. SIR-A over arid regions at nominal 1:1000000 scale; radar illumination is from approximately southward, i.e. from top of each image.

(*a*) Grand Kavir salt desert, north central Iran (data-take 28). Prominent but low-relief faulted anticlinal fold of mid-Tertiary continental sandstones and shales (producing alternate rough and smooth surfaces) apparently pierced by a salt-plug (not shown on geological maps). Surrounding areas are flat-lying Quaternary playas, silt and sand. Conspicuous salt plugs (Neogene) are especially well delineated by the L-band radar (right of image).

(*b*) Western Sahara (data-take 32/33). Remarkable sequence of regularly bedded Devonian arenaceous sediments showing minor faulting and drag-folding.

(*c*) Chaîne d'Ougarta, western Algeria (data-take 32/33). Cores of Upper Proterozoic sediments and volcanics surrounded by Lower Palaeozoic sediments. A dune field shows as a distinct black tone with dune features picked out by moderate backscatter from coarser materials and interdune areas.

(*d*) East of Ndjamena, Chad (data-take 28). Barchan-dune field derived from Lake Chad ancient deposits. Older long linear vegetated dunes can be seen at top right.

(*e*) West Queensland, Australia (data-take 35/36). Braided drainage of the Rivers Diamantina (left) and Hamilton (drains to Lake Eyre), crossing a mostly low-relief arid savannah underlain by Mesozoic platform-cover sediments outcropping at A. The bright tones of the drainage and outcrop results from radar backscatter from rough surfaces, in excess of a few centimetres trough-to-peak 'relief' according to Rayleigh formula. The black tones result from lack of backscatter from flat-lying waterlogged, and sand- and clay-covered, surfaces.

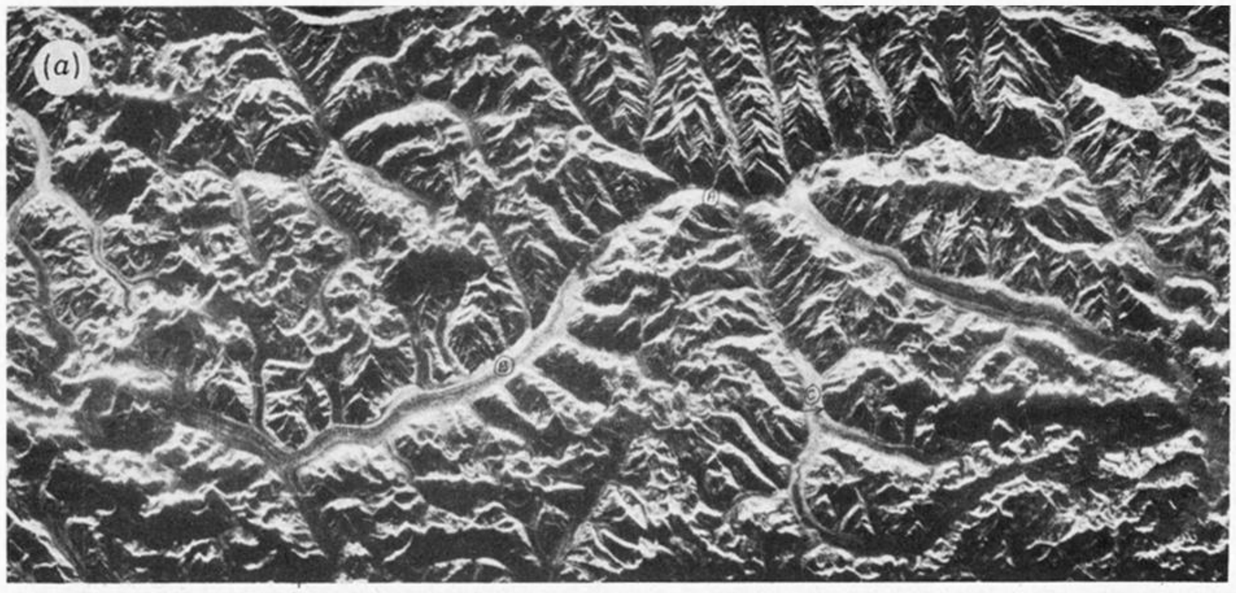

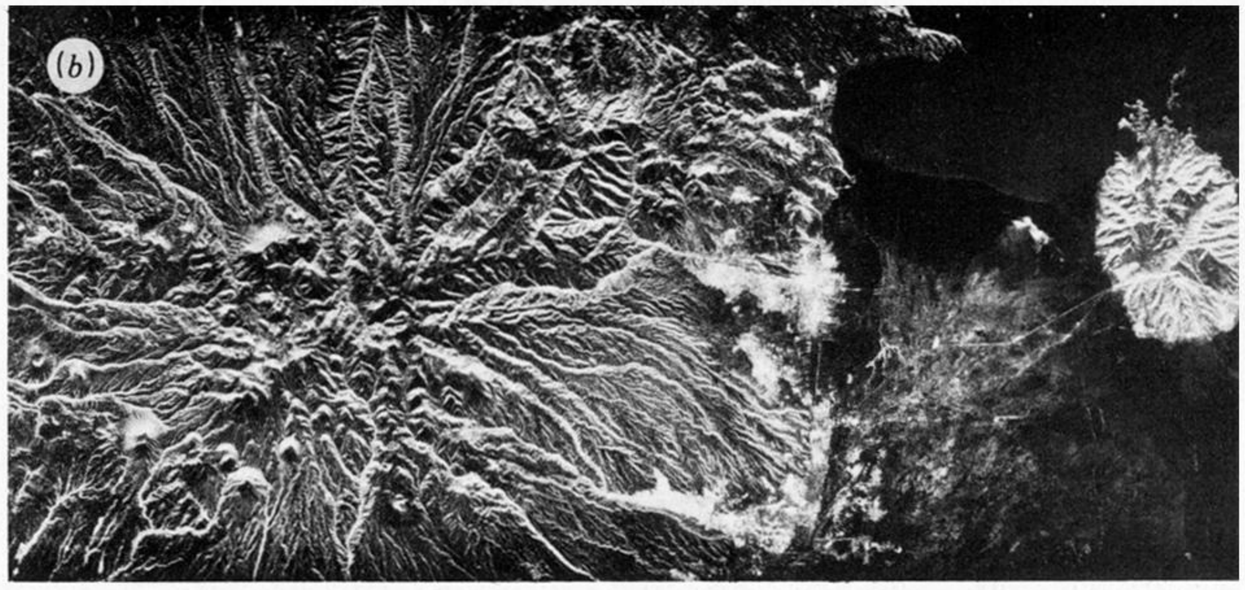

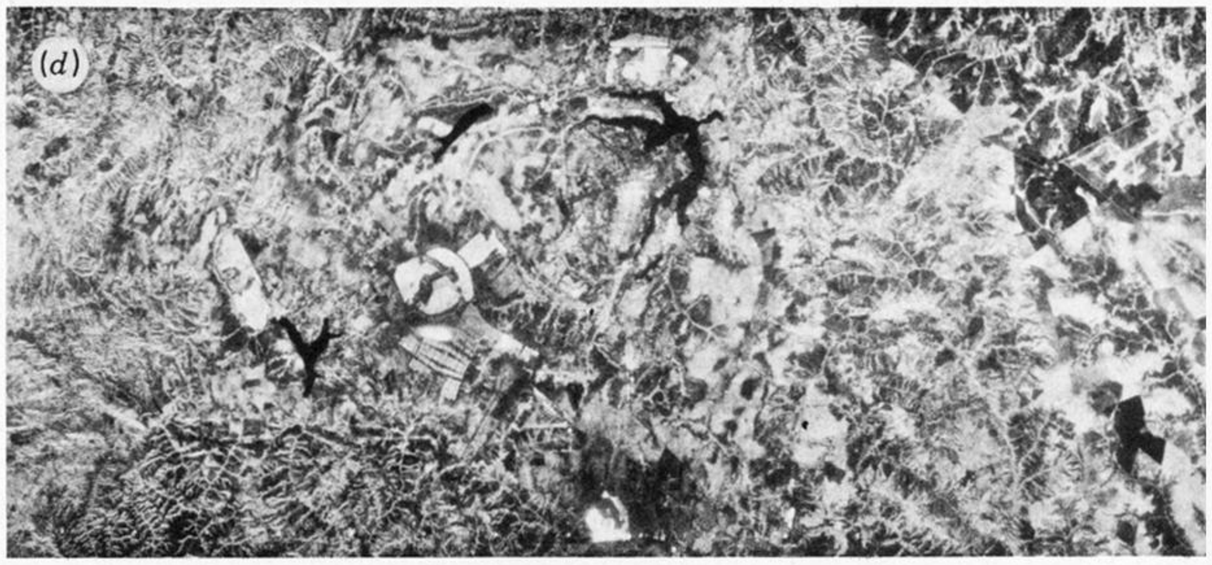

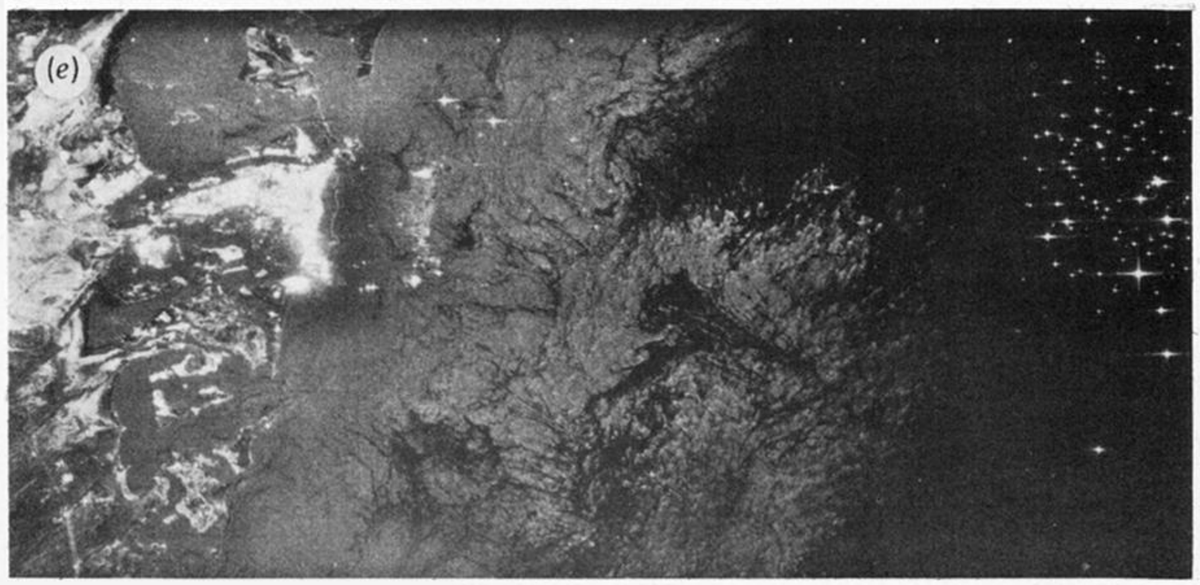

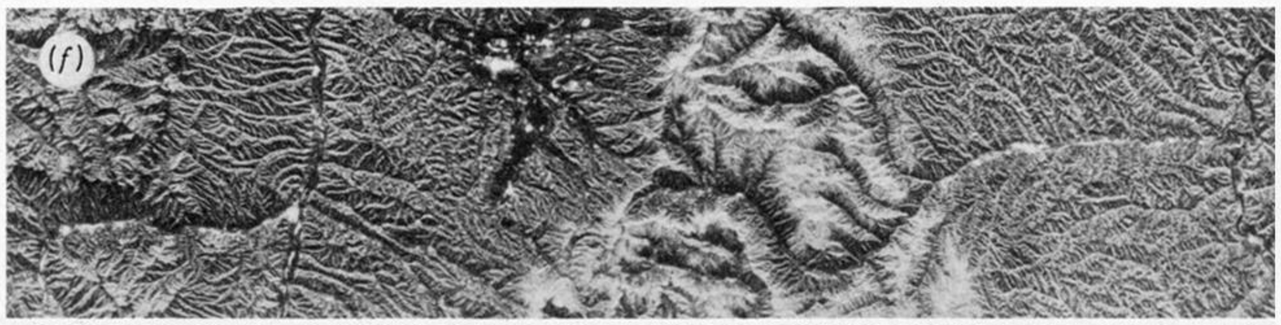

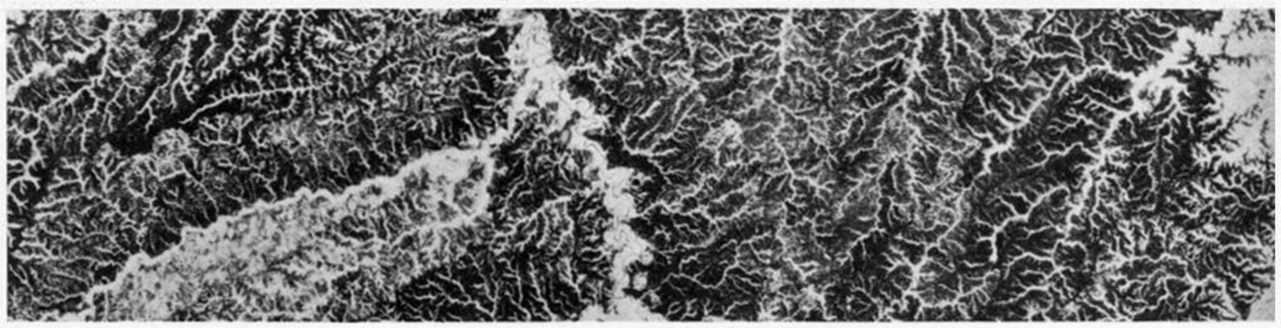

FIGURE 16. Topography, land use and coastal features on SIR-A imagery at nominal 1:1000000 scale; radar illumination is from southward, i.e. from top of each image.

(*a*) Karakoram Range, northwest Pakistan/southwest China (data-take 32/33). Peaks of typically 8000 m in the highest part of the Himalayas. Although lay-over and foreslope brightening are widespread and occasionally severe, there is little interfering radar shadow. The high altitude of the sensor results in an even illumination across the swath even in mountainous terrain; morphological detail, e.g. glaciers, is good although the content of bedrock geological data is poor. The thick snow of the whole area is apparently completely penetrated by the L-band radar.

(*b*) Kuh-e-Sahand/Boz Dagh (3700 m) volcano, Tabriz, northwest Iran (data-take 35/36). A massive Quaternary andesite volcano (over 5000 km²) with several cones, mostly of dacite. Tuffs and ashes occupy the lower slopes. The Kuh-e-Choruglu Neogene basalt volcano (on right) is surrounded by the lake of Daryacheh Yerezaiyeh (top right corner).

(*c*) Mexicali, northern Mexico (data-take 24C). Dense cultivation in semi-arid, low relief area showing fields, roads and towns, and marked difference of field patterns across the U.S. frontier to the north.

(*d*) Brasilia, eastern Brazil (data-take 24C). Roads, buildings, reservoirs, minor drainage channels, forest and cultivated areas show clearly in this example from tropical savannah.

(*e*) Arabian Gulf and Abu Dhabi (data-take 37A). Features offshore Abu Dhabi (large bright aggregate reflexions) include petroleum drilling rigs (bright stellate reflectors) and sea surface disturbance probably influenced by bottom topography.

(*f*) Examples of two dense drainage networks from Rio Meticá, Colombia (data-take 24C), and Shansi Graben, China, upper Huang-ho River (data-take 28).